Experimental Program Final Technical Report
15 February 2007 to 30 September 2012

Project Title: Intermediate Energy Nuclear Physics

US Dept. of Energy Grant No. DE-FG02-04ER41301

Principal Investigator: Edward R. Kinney, Professor Co-Principal Investigator: R. Jerome Peterson, Professor
Nuclear Physics Laboratory,
University of Colorado at Boulder

Contents

A. INTRODUCTION AND OVERVIEW

This report summarizes experimental work in basic nuclear physics carried out between October 16, 2006 and August 15, 2010 at the Nuclear Physics Laboratory of the University of Colorado, Boulder, under contract DE-FG02-04ER-41301 with the United States Department of Energy.

B. NUCLEON SPIN STRUCTURE AND EXCLUSIVE REACTIONS

1. The PHENIX Experiment

F. Ellinghaus, E.R. Kinney, J. Nuger, J. Seele, (University of Colorado), the PHENIX Collaboration.

The PHENIX experiment is one of two large collider experiments at RHIC that is designed to study both relativistic heavy ion collisions as well as high energy polarized proton collisions. The spectrometer consists of two logical units: forward spectrometers designed to detect muons, and central arms designed to detect photons, electrons, and hadrons. As is typical with these types of spectrometers there is a broad variety of physics questions which can be addressed, with major goals of determining the nature of the excited, dense matter created in heavy ion collisions, and determining the fraction of the proton spin carried by gluons.

In the 2005 run (Run-5), the first long polarized $p\,p$ run occurred, which has already produced numerous interesting results with a major advance in statistical precision. After funding was found, the 2006 run (Run-6) proceeded to produce a large sample of $p\,p$ data with high figure-of-merit. The Colorado spin group took an active part in the running and monitoring of the PHENIX experiment in the 2005 and 2006 runs, as well as in the heavy-ion run of 2007 and the short $p\,p$ and d-Au run of 2008. Preparation for Run-9 are underway at this writing; this run is expected to provide the first significant polarized $p\,p$ luminosity at 500 GeV collision energy.

A central process for determining the gluon contribution to the proton spin is inclusive hadron production from longitudinally polarized $p\,p$ collisions. At RHIC energies, where it appears that pQCD is a precise calculational technique, the inclusive hadron asymmetry can be determined from gg, gq and qq scattering. In the case of π^0 production at lowish p_T, the gg process is predominant, and so the asymmetry is sensitive to the square of the polarized gluon distributions of the nucleon.

Using the high statistics 2006 data set, the PHENIX collaboration has produced new results on the double spin asymmetry in π^0 production, which were published in *Physical Review Letters*. An empirical analysis compared to different model hypotheses for the gluon polarization shows that the new results constrain the gluon spin contribution to be very small or possibly negative. However, this conclusion is based on assumptions about the shape of the polarized gluon distribution in Bjorken x. Different shapes, especially those with zero crossings result in much less constraint.

The most recently released results are shown in Fig. 1.1 in which the double helicity asymmetry for inclusive π^0 production is compared to calculations based on various parameterizations of the polarized gluon distribution; the data are from Run-5 and Run-6. The right panel displays the result of a χ^2 analysis as a function of the total gluon contribution ΔG to the nucleon spin (again for

various assumptions about distribution shape). It clearly indicated that large positive values of ΔG are inconsistent with the data. These results have been submitted for publication [1].

The Colorado group has continued it analysis of the cross section and double helicity asymmetry in η meson inclusive production. These data should provide an important cross check of the interpretation of the π^0 asymmetry. A separate report follows below.

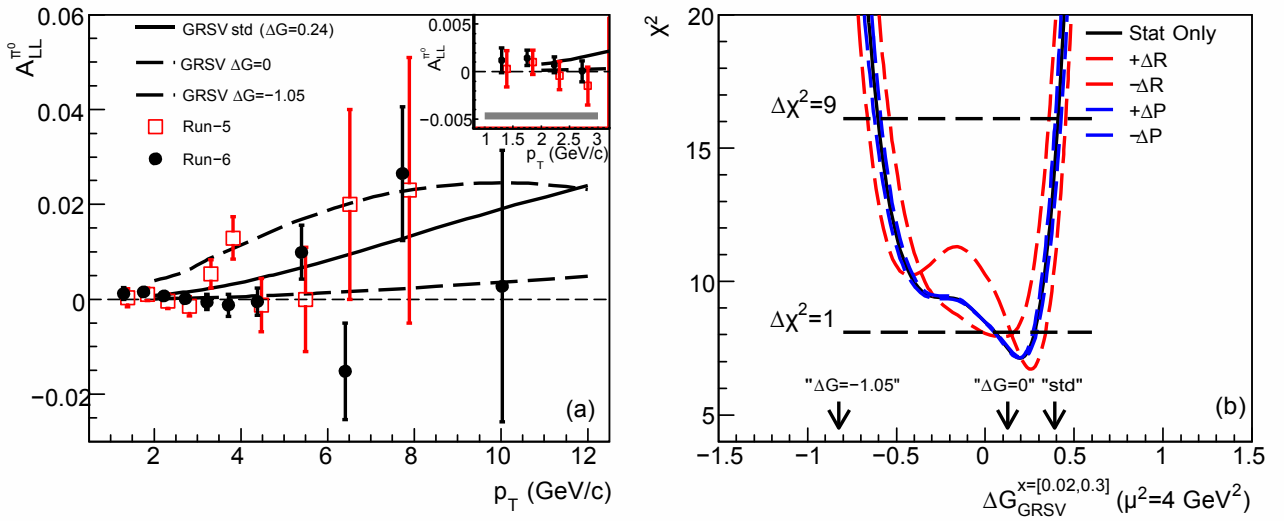

Figure 1.1: Left panel: Double spin asymmetry A_{LL} for inclusive π^0 production at mid-rapidity from polarized pp collisions at $\sqrt{s}$ = 200 GeV, as a function of transverse momentum of the π^0 (PHENIX), compared with calculations based on different parameterizations of the gluon polarized distribution. Right panel: The χ^2 distribution for fits of asymmetries from different polarized gluon parameterizations as a function of the total polarized gluon moment of the parameterization.

An upgrade of the PHENIX muon spectrometers so that the experiment can fully exploit the measurement of quark polarizations using *W* boson production is underway. After performing initial software simulations for feasibility studies, Prof. Nagle's group has continued to carry out electronic tests of RPC prototypes. Our activity has focused on the understanding of the quality of measurements of Z^0 bosons which can be made with the existing PHENIX spectrometer.While the yield of these bosons in Run-9 will be very small, the data are quite important, as they give us a first glimpse of what the hadronic backgrounds will be for the physics measurement. Analysis and comparison to simulation will be a critical task in the next year.

References

[1] A. Adare *et al.,* arXiv:0810.0694, Phys. Rev. Lett. (under review).

1.a Double Longitudinal Helicity Asymmetry and Cross Section for mid-rapidity η production in polarized p+p collisions at $\sqrt{s}$ = 200 GeV

J. Seele, F. Ellinghaus, E. Kinney (University of Colorado), the PHENIX Collaboration.

The double longitudinal helicity asymmetry for mid-rapidity η production in polarized *pp* collisions at $\sqrt{s}$ = 200GeV provides information about the gluon helicity structure of the proton, since the asymmetry can be related, through perturbative QCD and the assumption of factorization, to the fundamental *gg*, *gq*, and *qq* polarized scattering processes. The reproduction of the inclusive π^0 cross section at this CM energy [1], over many orders of magnitude, suggests that one is well into the energy region where pQCD can be used with precision. In the case of the η, the statistics are significantly smaller, but the Run-5 and Run-6 data sets are sufficient to determine cross section and asymmetry with good precision. In addition, the η fragmentation function has been determined via global fits to the world e^+e^- and *pp* data [4].

The η Reconstruction, Cross Section and Asymmetry Determination The central arms of the PHENIX spectrometer [5] are used to reconstruct the photons from the 2 photon decay channel of the η. The branching ratio for this decay channel is .3938 [6]. Because of the geometry of the PHENIX central arms, the acceptance is limited at low transverse momentum (p_T). The PHENIX electromagnetic calorimeter is used to obtain the momentum and energy of the photons, the pad chamber is used to veto charged tracks, and the beam-beam counters are used to locate the interaction vertex. For the reconstruction, a high p_T electromagnetic trigger is required by one of the photons which contributed to the correct invariant mass. This allows an integrated luminosity to be calculated for the measurement.

The integrated luminosity of the high p_T electromagnetic trigger is calculable through a relation to the minimum bias trigger which, through simulations, is related to total inelastic cross section of 22.6 mb. The η cross section, as a function of p_T, can then be calculated to cross check the helicity measurement as well as to see if the cross section is well described by perturbative QCD.

The helicity asymmetry is defined as

$$A_{LL} = \frac{1}{P_B P_Y} \frac{\frac{N_{++}}{L_{++}} - \frac{N_{+-}}{L_{+-}}}{\frac{N_{++}}{L_{++}} + \frac{N_{+-}}{L_{+-}}} = \frac{\sigma_{++} - \sigma_{+-}}{\sigma_{++} + \sigma_{+-}} = \frac{\Delta\sigma}{\sigma} \quad (1)$$

where the N_{++} (N_{+-}) and L_{++} (L_{+-}) are the counts and integrated luminosities in a given period of data taking. From the above equation, the necessity of the measurement of the cross section can also be seen if the extraction of the cross section helicity difference is to be undertaken, rather than just the asymmetry. For this measurement the same trigger is applied as in the case of the cross section

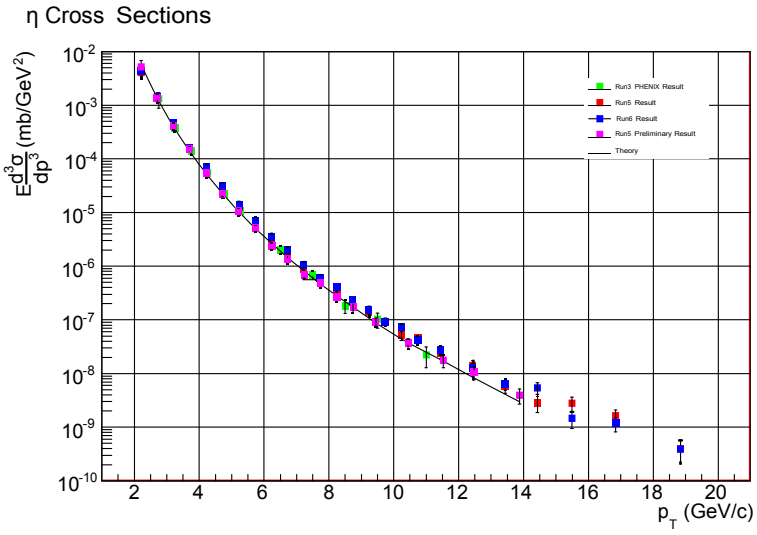

Figure 1a.1: PHENIX Preliminary inclusive η cross section at central rapidity as a function of p_T from PHENIX runs 3, 5, and 6, compared with the prediction based on the new η fragmentation functions.

measurement to provide an experimental cross-check. The Run-5 and Run-6 preliminary results for the cross section are shown in Fig. 1a.1.

From these *pp* data, along with η yields form e^+e^- collisions, new η fragmentation functions have been fit, as shown in Fig. 1a.2. These fragmentation functions are critical input to the calculation of the double helicity asymmetry using the also the (known) polarized quark distributions and different models of the polarized gluon distribution.

The Run-5 and Run-6 preliminary results for the double helicity asymmetry A_{LL} are shown in Fig. 1a.3 compared with predictions [3] with the GRSV polarized distributions [2], using the new η fragmentation functions. The results are consistent with those from inclusive π^0 asymmetries.

Now that the Run-6 analysis is complete, a manuscript presenting the results is in preparation and is expected to be submitted to a journal sometime in spring 2009.

References

[1] B. Jager, A. Schafer, M. Stratmann and W. Vogelsang, Phys. Rev. D **67**, 054005 (2003).

[2] M. Glück, E. Reya, M. Stratmann, W. Vogelsang, Phys. Rev. D **63**, 094005 (2001).

[3] M. Stratmann, W. Vogelsang, private communication (2007).

[4] C. Aidala, J.Seele, M. Stratmann, and W. Vogelsang, Bull. Am. Phys. Soc. **52** (2007).

[5] K. Adcox *et al.*, Nucl. Instrum. Meth. A **499**, 469 (2003).

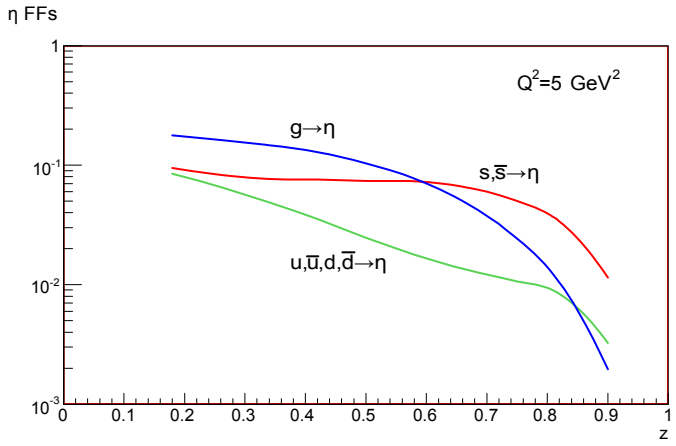

Figure 1a.2: A set of the η fragmentation functions at a scale of $\mu^2 = 5$ GeV^2 as a function of z, the fraction of original parton energy carried by the final hadron resulting from the fragmentation process.

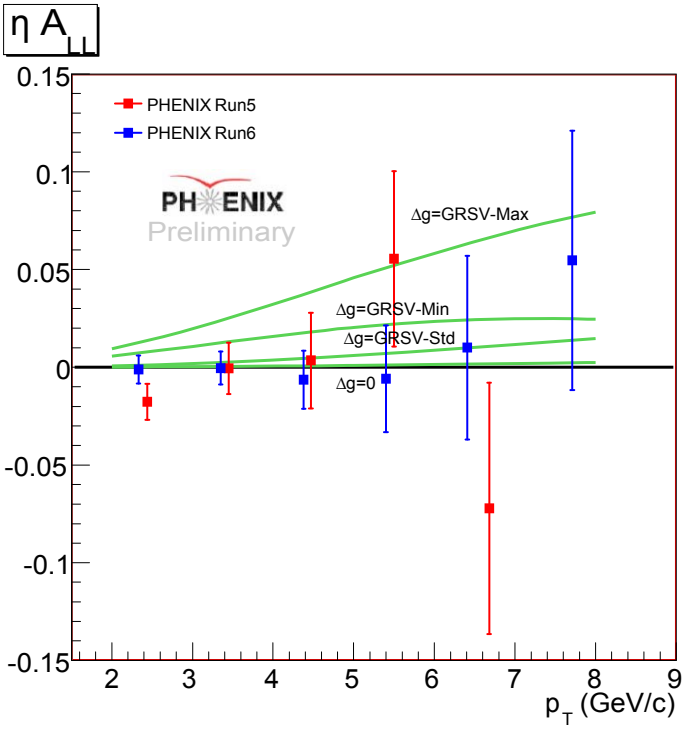

Figure 1a.3: PHENIX Preliminary A_{LL} for Run-5 and Run-6 as a function of p_T, compared with calculations using different models for the polarized gluon distributions.

[6] C. Amsler *et al.,* Phys. Lett. B **667**, 1 (2008).

1.b Realistic Simulation of Z^0 Boson Production in the PHENIX Muon Spectrometers

E.R. Kinney, and J. Nuger (University of Colorado)

The separate contributions of $\bar{u}$ and $\bar{d}$ quarks to the proton spin are at present known only from lepton SIDIS (Semi-Inclusive Deep Inelastic Scattering) double spin asymmetries, in which they are extracted using the "hadron tagging" technique. Single spin asymmetries of leptons from W bosons produced in longitudinally polarized $p\,p$ collisions are directly sensitive to the sea quark polarizations, without having to understand any final hadronic states [1]. The PHENIX collaboration at RHIC plans to determine the W^+ and W^- boson production cross sections and single spin asymmetries at $\sqrt{s}$ = 500 GeV by detecting decay muons at forward and backward rapidities. In order
to understand resolution, backgrounds, and efficiency effects, the PHENIX spectrometer simulation PISA was used to studied the planned measurements and determine realistic expectations of the yields and the sensitivity to the light quark polarizations. The $W^{\pm}$ events themselves were generated using the PYTHIA code. These studies indicated that the present spectrometer resolution will limit our ability to determine the x dependence of the polarized distributions [2].

An important test of the resolution and means of calibration is the detection of the $\mu^+\mu^-$ decay of Z^0 bosons. The absolute cross section for this process is of intrinsic interest as well. Comparison with the W cross section at forward and backward rapidity constrains the unpolarized light sea quark distributions. Starting in Fall 2008, we have begun simulation studies of the $Z^0 \rightarrow \mu^+\mu^-$ production and detection in the PHENIX spectrometer, again using the realistic PISA spectrometer model. We expect to complete these studies in Spring 2009.

References

[1] G. Bunce *et al., Ann. Rev. Nucl. Part. Sci.* **50** 525 (2000).

[2] K.G. Kiriluk, "Simulation of W Boson Production in the PHENIX Muon Spectrometers," Masters Thesis (unpublished) (2007).

2. The HERMES Experiment

F. Ellinghaus, E.R. Kinney, A. Martinez de la Ossa (University of Colorado), The HERMES Collaboration

The HERMES experiment is designed to use deep inelastic scattering of polarized electrons from polarized targets to study the quark spin distributions within the nucleon. Earlier experiments found that only 30-40% of the nucleon spin is carried by the quarks, which is surprising given the simple explanation of the baryon static magnetic moments in terms of simple quark spin wavefunctions. In general, one expects the spin to arise from the spins of the up, down, and strange quarks, ΔU, Δd, and Δs respectively, as well as a contribution from the gluonic field ΔG and the angular momentum of the quarks L_q, as shown in the follow heuristic formula:

$$\frac{1}{2} = \frac{1}{2}(\Delta u + \Delta d + \Delta s) + \Delta G + L_q.$$

Inclusive lepton scattering basically determines the sum from the quark spins only, though there is a contribution coming from the gluons via the axial anomaly. In fact, in the simple quark model, the spin structure function g_1 is just the difference between the distributions of quarks polarized parallel and anti-parallel to the nucleon spin, summed over the quark flavors. These distributions are function of Bjorken x which can be thought of as the momentum fraction of the nucleon carried by the quark (strictly true in the infinite momentum frame).

HERMES has moved beyond inclusive measurements because of its use of an open geometry spectrometer instrumented to identify hadrons as well as the scattered leptons. This allows the measurement of so-called semi-inclusive reactions where a high energy hadron is detected in coincidence with the scattered lepton, as shown schematically in Fig. 2.1

Since the hadron type is correlated with the type of quark which absorbed the virtual photon, one can deduce the fraction of the quark spin carried by the various quark flavors. A highlight of this year's activity was the publication [1] of a new analysis of the unpolarized and polarized $s + \bar{s}$ quark distribution, using semi-inclusive $K^+ + K^-$ multiplicities and asymmetries from longitudinally polarized deuterons. This purely isoscalar analysis avoids having to model all the distributions, since the multiplicities are used to empirically determine the necessary unpolarized distributions.

Figure 2.2 shows the results for the $S(x) \equiv s(x) + \bar{s}(x)$ distribution determined from the data; it is significantly softer than standard models of the sea distributions. Figure 2.3 shows the resulting non-strange and strange helicity distributions, compared to a parameterization of world data by Leader [2]. As in previous analyses, the HERMES data are consistent with zero or slightly positive strange quark polarization, at least in the intermediate region of x to which HERMES is sensitive. This is in sharp contrast to the overall negative contribution expected from the inclusive g_1 result combined

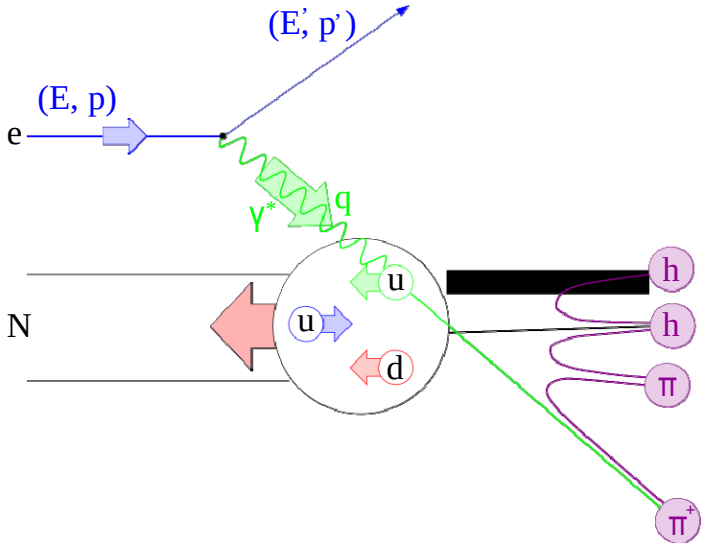

Figure 2.1: Schematic of a deep inelastic scattering reaction.

with an SU(3) flavor symmetric analysis of baryon moments. A recent parameterization [3] which includes these data as well as the double spin asymmetries from the RHIC spin program, allows for a slightly positive S in this x range, but must balance this with a negative polarization at very low x.

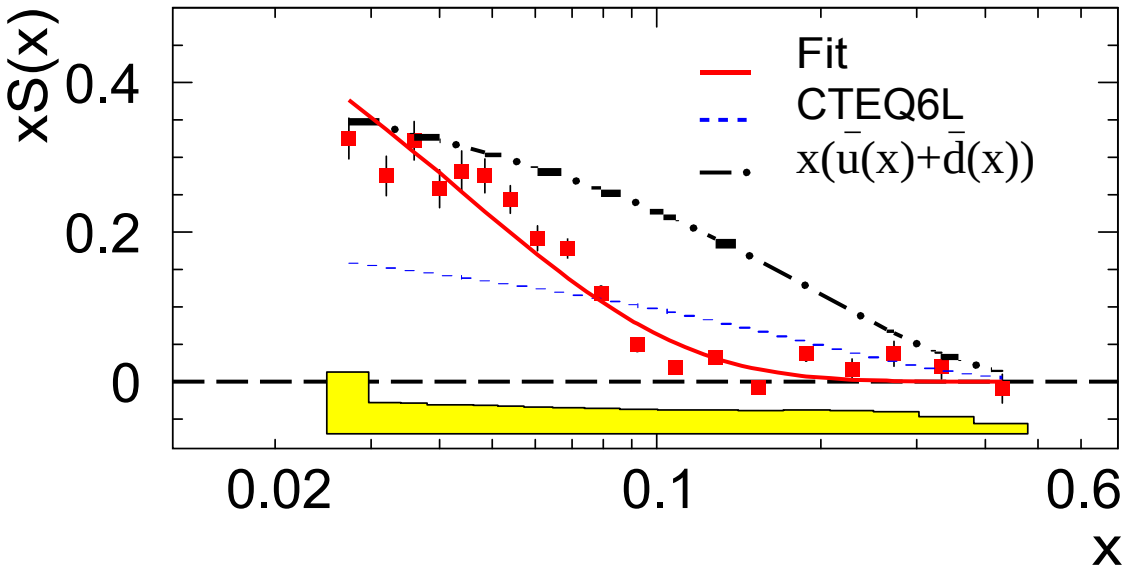

Figure 2.2: The strange parton distribution from the measured HERMES multiplicity for charged kaons evolved at Q^2 = 2.5 GeV^2

New exclusive analyses continue to be completed from the pre-recoil era of HERMES running. In spring 2008 a new combined extraction of deeply virtual compton scattering (DVCS) amplitudes

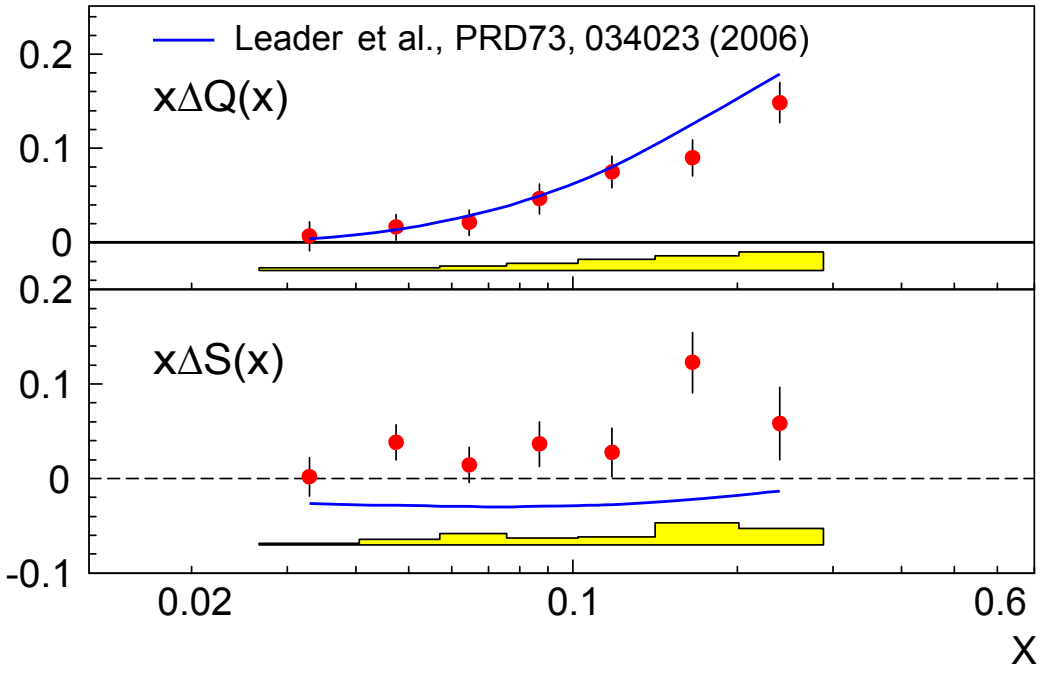

Figure 2.3: Non-strange and strange quark helicity distributions at Q^2 = 2.5 GeV^2, as a function of Bjorken x. The curves are the LO results from Leader *et al.* [2] from their analysis of world data.

using both beam spin and charge information allowed the first extraction of the spin-charge interference moment. In the area of semi-inclusive physics with a transverse target polarization two new preliminary results have been released in September 2008 that are quite exciting: the so-called Cahn moment, a direct result of transverse motion of quarks, and the Boer-Mulders moment which probes the correlation between quark spin and quark transverse (orbital) motion. This latter is an exciting first direct glimpse of a spin-orbit interaction in the current quark regime, rather than the constituent quark model.

Meanwhile the first complete calibration of the recoil spectrometer detectors was completed in August 2008, and now the physics analysis of the very large data set can be started. First results are expected by summer 2009. The DESY management continues to strongly support the final analysis phases of HERMES, which are expected to continue over the next 4 years.

References

[1] A. Airapetian *et al.,* Phys. Lett. B **666**, 446 (2008).

[2] E. Leader *et al.,* Phys. Rev. D **73** 034023 (2006).

[3] D. de Florian, R. Sassot, M. Stratmann, and W. Vogelsang, Phys. Rev. Lett. **101**, 072001 (2008).

2.a Implementation of Magnetic Field Correction in HERMES Vertex Region

A. Martinez de la Ossa (University of Colorado)

During the running of the HERMES experiment with a transversely polarized target, stray fields from the target magnet cause low momentum tracks to bend slightly resulting in a degradation of spectrometer momentum resolution and vertex location. Field measurements were taken in this drift region and codes to account for the effect of these fields on the charged particles were developed and implemented in the standard HERMES analysis software. As a demonstration of the improvement in resolution, Fig. 2a.1 shows the invariant mass spectrum of $\pi^+\pi^-$ pairs from the data set collected in 2006-2007, in the region of the K_S peak; this should be compared with Fig. 2a.2, which shows the same spectra using the new field correction codes and demonstrated a clear reduction in peak width. Unfortunately, it also appears to introduce a shift of the centroid away from the correct value; this is being investigated further.

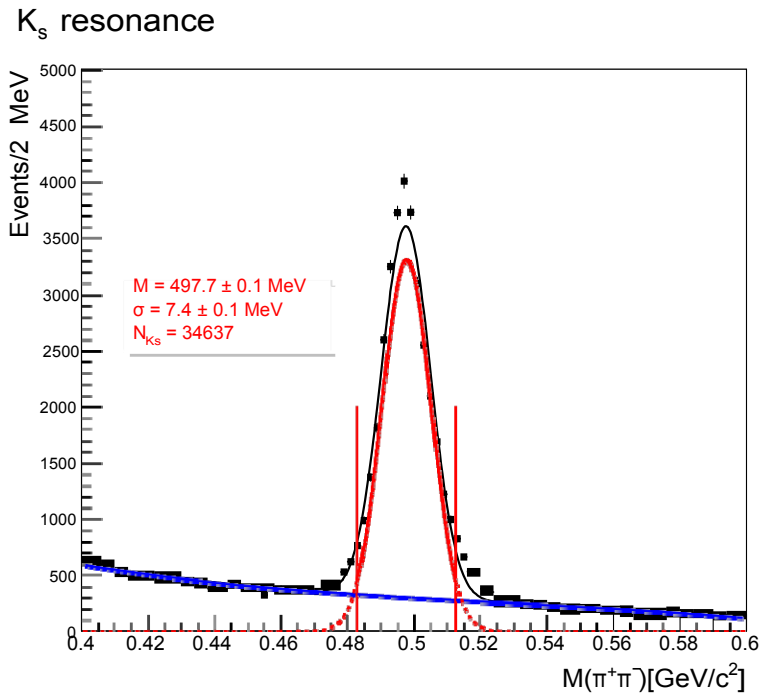

Figure 2a.1: Invariant mass spectrum of $\pi^+\pi^-$ pairs from the HERMES 2006-2007 data set in the region of the K_S particle mass. The momenta of the pions was calculated without the target magnet field corrections.

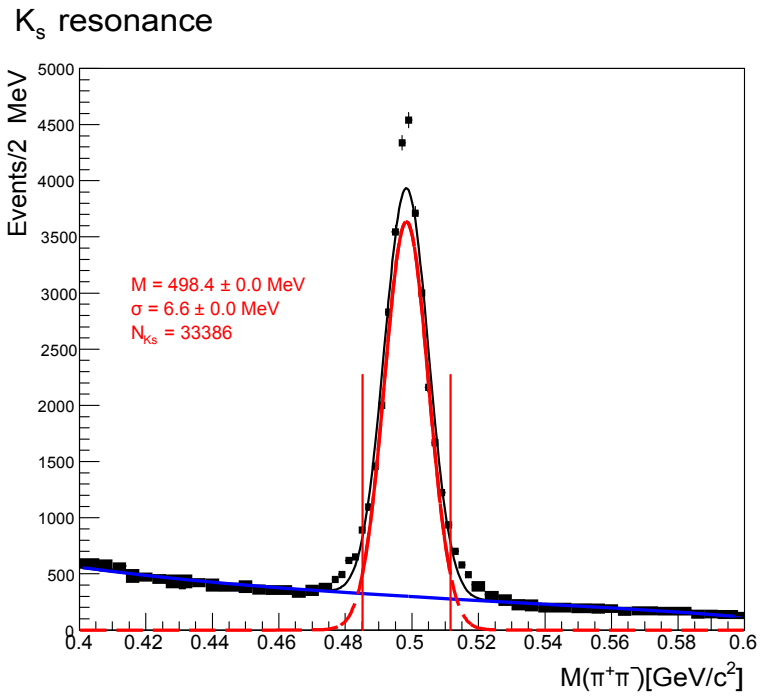

Figure 2a.2: Invariant mass spectrum of $\pi^+\pi^-$ pairs from the HERMES 2006-2007 data set in the region of the K_S particle mass. The momenta of the pions was calculated with the new target magnet field corrections.

2.b Search for a Two-Photon Exchange Contribution to Inclusive Deep-Inelastic Scattering

A. Martinez de la Ossa (University of Colorado)

Introduction In recent years, the contribution of two-photon exchange to the cross section for electron-nucleon scattering has received considerable attention. In elastic $e\,p$ scattering, two-photon exchange effects are believed to be the best candidate to explain the discrepancy in the measurement of the ratio G_E/G_M of the electric and magnetic form factors of the proton obtained at large four-momentum transfer between the Rosenbluth method and the polarization transfer method [1]. It has been shown that the interference between the one-photon and two-photon exchange amplitudes can affect the Rosenbluth extraction of the nucleon form factors at the level of a few percent. This is enough to explain most of the discrepancy between the results of the two methods [2, 3], although none of the recent calculations can fully resolve the discrepancy at all momentum transfers [4]. Two-photon exchange effects have also been shown to affect the measurement of parity violation in elastic scattering of longitudinally polarized electrons off unpolarized protons, with corrections of several percent to the parity-violating asymmetry [5].

In order to investigate contributions from two-photon exchange, it is necessary to find experimental observables that allow their isolation. Beam-charge and transverse single-spin asymmetries (SSAs) are two suitable candidates. In both elastic and inclusive inelastic lepton-nucleon scattering, these asymmetries arise from the interference of one-photon and two-photon exchange amplitudes. Specifically, beam-charge asymmetries in the unpolarized cross section arise from the real part of the two-photon exchange amplitude [6], while inclusive transverse SSAs are sensitive to the imaginary part [7].

To date, all evidence of non-zero two-photon exchange effects in lepton-nucleon interactions comes from elastic scattering, $l+N \rightarrow l^{i}+N^{i}$. Measurements of the cross-section ratio $R = \sigma_{e^+p}/\sigma_{e^-p}$ are compiled in Ref. [6]. Though the individual measurements are consistent with R being unity, a recent reanalysis [8] demonstrates that a deviation of about 5% at low values of four-momentum transfer and virtual-photon polarization is not excluded. Three experiments have measured a non-zero transverse-beam SSA of order $10^{-5}-10^{-6}$ in elastic scattering of transversely polarized electrons off unpolarized protons [9–11].

In inelastic scattering no clear signature of two-photon exchange effects has yet been observed. Measurements of the cross-section ratio R with e^+/e^- and μ^+/μ^- beams [12–18] show no effect within their accuracy of a few percent. The transverse-target SSA has been measured at the Cambridge Electron Accelerator [19, 20] and at scatteringSlac [21]. The data are confined to the region of nucleon resonances, and show an asymmetry which is compatible with zero within the few-percent

level of the experimental uncertainties.

In inclusive deep-inelastic scattering (DIS), $l + p \rightarrow l' + X$, and in the one-photon exchange approximation, such a SSA is forbidden by the combination of time reversal invariance, parity conservation, and the hermiticity of the electromagnetic current operator, as stated in the Christ-Lee theorem [22]. A non-zero SSA can therefore be interpreted as an indication of two-photon exchange.

Ref. [7] presents a theoretical treatment of the transverse SSA arising from the interference of one-photon and two-photon exchange amplitudes in DIS. For an unpolarized beam (U) and a transversely (T) polarized nucleon target, the spin-dependent part of the cross section is given by

$$\sigma_{UT} \propto e_l \alpha_{em} \frac{M}{Q} \varepsilon_{\mu\nu\rho\sigma} S^{\mu} p^{\nu} k^{\rho} k'^{\sigma} C_T. \qquad (2)$$

Here, e_l is the charge of the incident lepton, M is the nucleon mass, $-Q^2$ is the squared four-momentum transfer, p, k and k' are the four-momenta of the target, the incident and the scattered lepton, respectively, while $\varepsilon_{\mu\nu\rho\sigma}$ is the Levi-Civita tensor. The term $\varepsilon_{\mu\nu\rho\sigma} S^{\mu} p^{\nu} k^{\rho} k'^{\sigma}$ is proportional to $\vec{S} \cdot (\vec{k} \times \vec{k}')$, consequently the largest asymmetry is obtained when the spin vector $\vec{S}$ is perpendicular to the lepton scattering plane defined by the three-momenta $\vec{k}$ and $\vec{k}'$. Finally, C_T is a higher-twist term arising from quark-quark and quark-gluon-quark correlations.

As σ_{UT} is proportional to the electromagnetic coupling constant α_{em}, it is expected to be small. Furthermore, due to the factor M/Q in Eq. (2), σ_{UT} is expected to increase with decreasing Q^2. A calculation based on certain model assumptions [23] for a scatteringJlab experiment [24] yields expectations for the asymmetry of order 10^{-4} at the kinematics of that experiment. The authors in Ref. [7], on the other hand, do not exclude asymmetries as large as 10^{-2} and point out that the term C_T in Eq. (2) cannot be completely evaluated at present. Due to the factor e_l in Eq. (2), the asymmetry is expected to have a different sign for opposite beam charges. The capability of the scatteringHera accelerator to supply both electron and positron beams thus provides an additional means to isolate a possible effect from two-photon exchange.

In this work a first precise measurement of the transverse-target SSA in inclusive DIS of unpolarized electrons and positrons off a transversely polarized hydrogen target is presented.

The analysis The data were collected with the scatteringHermes spectrometer [25] during the period 2002-2005. The 27.6 GeV positron or electron beam was scattered off the transversely polarized gaseous hydrogen target internal to the scatteringHera storage ring at scatteringDesy. The open-ended target cell was fed by an atomic-beam source [26] based on Stern-Gerlach separation combined with radio-frequency transitions of hydrogen hyperfine states. The direction of the target spin vector was reversed at 1-3 minute time intervals to minimize systematic effects, while both the nuclear polarization and the atomic fraction of the target gas inside the storage cell were continuously measured [27]. Data were collected with the target polarized transversely to the beam direction, in

both “upward” and “downward” directions in the laboratory frame. The beam was longitudinally polarized, but a helicity-balanced data sample was used to obtain an effectively unpolarized beam. Only the scattered leptons were considered in this analysis. Leptons were distinguished from hadrons by using a transition-radiation detector, a scintillator pre-shower counter, a dual-radiator ring-imaging Cherenkov detector, and an electromagnetic calorimeter. Hadrons were suppressed by very stringent particle identification requirements to a level of less than 2×10^{-4} to exclude any contamination from a possible transverse hadron SSA in the lepton signal. This resulted in a lepton identification efficiency greater than 94%. Events were selected in the kinematic region $0.007 < x_B < 0.9$, $0.1 < y < 0.85$, $0.25\ \mathrm{GeV}^2 < Q^2 < 20\ \mathrm{GeV}^2$, and $W^2 > 4\ \mathrm{GeV}^2$. Here, x_B is the Bjorken scaling variable, y is the fractional beam energy carried by the virtual photon in the laboratory frame, and W is the invariant mass of the photon-nucleon system.

The differential yield for a given target spin direction ($\uparrow$ upwards or $\downarrow$ downwards) can be expressed as

$$\frac{d^3N^{\uparrow(\downarrow)}}{dx_B\,dQ^2\,d\varphi_S} = \int L^{\uparrow(\downarrow)}\, d^3\sigma_{UU} + (-) L_P^{\uparrow(\downarrow)}\, d^3\sigma_{UT} \Big] \Omega(x_B, Q^2, \varphi_S)$$
$$= d^3\sigma_{UU} \int L^{\uparrow(\downarrow)} + (-) L_P^{\uparrow(\downarrow)} A_{UT}^{\sin\varphi_S}(x_B, Q^2) \sin\varphi_S \Big] \Omega(x_B, Q^2, \varphi_S). \quad (3)$$

Here, φ_S is the azimuthal angle about the beam direction between the lepton scattering plane and the “upwards” target spin direction, σ_{UU} is the unpolarized cross section. Also, $L^{\uparrow(\downarrow)}$ is the total luminosity in the $\uparrow$ ($\downarrow$) polarization state, $L_P^{\uparrow(\downarrow)}$ is the luminosity weighted by the magnitude P of the target polarization, and Ω is the detector acceptance efficiency. The $\sin\varphi_S$ azimuthal dependence follows directly from the form $\vec{S} \cdot (\vec{k} \times \vec{k}')$ of the spin-dependent part of the cross section.

The asymmetry was calculated as

$$A_{UT}(x_B, Q^2, \varphi_S) = \frac{\frac{N^{\uparrow}}{L_P^{\uparrow}} - \frac{N^{\downarrow}}{L_P^{\downarrow}}}{\frac{N^{\uparrow}}{L^{\uparrow}} + \frac{N^{\downarrow}}{L^{\downarrow}}}, \quad (4)$$

where $N^{\uparrow(\downarrow)}$ are the number of events measured in bins of x_B, Q^2, and φ_S.

With the use of Eq. (3), it can be approximated, for small differences of the two average target polarizations ($P^{\uparrow}$) and ($P^{\downarrow}$), as

$$A_{UT}(x_B, Q^2, \varphi_S) \quad A_{UT}^{\sin\varphi_S} \sin\varphi_S + \frac{1}{2} \frac{(P^{\downarrow}) - (P^{\uparrow})}{(P^{\uparrow})(P^{\downarrow})}. \quad (5)$$

As shown in Table 2b.1, ($P^{\uparrow}$) and ($P^{\downarrow}$) are the same to a good approximation for all data-taking periods.

year	beam	$\langle P^{\uparrow} \rangle$	$\langle P^{\downarrow} \rangle$	Events
2002	e^+	0.783±0.041	0.795±0.041	0.9 M
2004	e^+	0.745±0.054	0.742±0.054	2.0 M
2005	e^-	0.705±0.065	0.705±0.065	4.8 M

Table 2b.1: Average target polarizations and total number of inclusive events for the three data sets used in this analysis.

The advantage of using the fully-differential asymmetry $A_{UT}(x_B, Q^2, \varphi_S)$ in Eq. (4) instead of the more common left-right asymmetry $A_N(x_B, Q^2)$ is that the acceptance function Ω cancels in each (x_B, Q^2, φ_S) kinematic bin, if the bin size or the asymmetry is small. Assuming the φ_S dependence of σ_{UT} in Eq. (2) and Eq. (3), the $\sin\varphi_S$ amplitude $A_{UT}^{\sin\varphi_S}$ and the left-right normal asymmetry A_N are related by

$$A_N = \frac{\int_0^{\pi} d\varphi_S \; d^3\sigma_{UU} \, A_{UT}^{\sin\varphi_S} \; \sin\varphi_S}{\int_0^{\pi} d\varphi_S \; d^3\sigma_{UU}} = \frac{2}{\pi} A_{UT}^{\sin\varphi_S} . \qquad (6)$$

For this analysis the Q^2 range was divided into a "DIS region" with $Q^2 > 1$ GeV^2 (denoted by closed circles in Fig. 2b.1) and a "low-Q^2 region" with $Q^2 < 1$ GeV^2 (denoted as open circles). To test for a possible enhancement of the transverse-target SSA due to the factor M/Q appearing in Eq. (2) the data at low Q^2 are also shown, though, strictly speaking, Eq. (2) may not be applicable to this range.

Due to the kinematics of the experiment, the quantities x_B and $\langle Q^2 \rangle$ are strongly correlated, as shown in the bottom panel of Fig. 2b.1.

The $A_{UT}^{\sin\varphi_S}$ amplitudes were extracted with a binned χ^2 fit of the functional form $p_1 \sin\varphi_S + p_2$ to the measured asymmetry. Leaving p_2 as a free parameter or fixing it to the values given by Eq. (5) and Table 2b.1 had no impact on the extracted $\sin\varphi_S$ amplitude $p_1 \equiv A_{UT}^{\sin\varphi_S}$.

Results The resulting amplitudes were not corrected for smearing or contamination by the radiative tail from elastic scattering; the latter correction requires knowledge of the presently unknown elastic two-photon asymmetry. Instead, the contribution of the elastic radiative tail to the total event sample was estimated from a Monte Carlo simulation based on the scatteringLepto generator [28] together with the scatteringRadgen [29] determination of QED radiative effects and with a scatteringGeant [30] based simulation of the detector. The elastics fraction is shown in the lower panel of Fig. 2b.1, it reaches values as high as about 35% in the lowest x_B bin, and rapidly decreases towards high x_B, becoming less than 3% for $x_B > 0.1$.

The final results for the measured $\sin\varphi_S$ amplitudes $A_{UT}^{\sin\varphi_S}$ are shown in Fig. 2b.1 as a function of x_B separately for electrons and positrons. In both cases the asymmetries are consistent with zero within their uncertainties.

The systematic uncertainties, shown in the fourth column of Table II and as error boxes in Fig. 2b.1, include contributions due to corrections for misalignment of the detector, beam position and slope at the interaction point and bending of the beam and the scattered lepton in the transverse holding field of the target magnet. They were determined from a high statistics Monte Carlo sample obtained from a simulation containing a full description of the detector, where an artificial spin-dependent azimuthal asymmetry was implemented. Input asymmetries being zero or as small as 10^{-3} were well reproduced within the statistical uncertainty of the Monte Carlo sample, which was about five times smaller than the statistical uncertainty of the data. For each measured point the systematic uncertainty was obtained as the maximum value of either the statistical uncertainty of the Monte Carlo sample or the difference between the input asymmetry and the extracted one. Systematic uncertainties from other sources like particle identification or trigger efficiencies were found to be negligible.

The transverse single-spin asymmetry amplitudes $A_{UT}^{\sin\varphi_S}$ for electron and positron beams integrated over x_B are given separately for the "low-Q^2 region" and the "DIS region" in Table 2b.2 along with their statistical and systematic uncertainties. All asymmetry amplitudes are consistent with zero within their uncertainties, which in the DIS region are of order 10^{-3}. The only exception is the low-Q^2 electron sample, where the asymmetry is 1.9 standard deviations different from zero. No hint of a sign change between electron and positron asymmetries is observed within uncertainties.

beam	$A_{UT}^{\sin\varphi_S}$ $\times 10^{-3}$	$\delta A_{UT}^{\sin\varphi_S}$(stat.) $\times 10^{-3}$	$\delta A_{UT}^{\sin\varphi_S}$(syst.) $\times 10^{-3}$	$\langle x_B \rangle$	$\langle Q^2 \rangle$ [GeV^2]
e^+	-0.61	3.97	0.63	0.02	0.68
e^-	-6.55	3.40	0.63		
e^+	-0.60	1.70	0.29	0.14	2.40
e^-	-0.85	1.50	0.29		

Table 2b.2: The integrated transverse single-spin asymmetry amplitude $A_{UT}^{\sin\varphi_S}$ with its statistical and systematic uncertainties and the average values for x_B and Q^2 measured separately for electron and positron beams in the two Q^2 ranges $Q^2 < 1$ GeV^2 (upper rows) and $Q^2 > 1$ GeV^2 (lower rows). The systematic uncertainties contain the effects of detector misalignment and beam position and slope at the target, as estimated by a Monte Carlo simulation, but not the scale uncertainties from the target polarization which amounts to 9.3% (6.6%) for the electron (positron) sample. Also, the results are not corrected for smearing, radiative effects and elastic background events.

Conclusion In conclusion, single-spin asymmetries were measured in inclusive deep-inelastic scattering at scatteringHermes with unpolarized electron and positron beams and a transversely polarized hydrogen target with the goal of searching for a signal of two-photon exchange. No signal was found within the uncertainties, which are of order 10^{-3}.

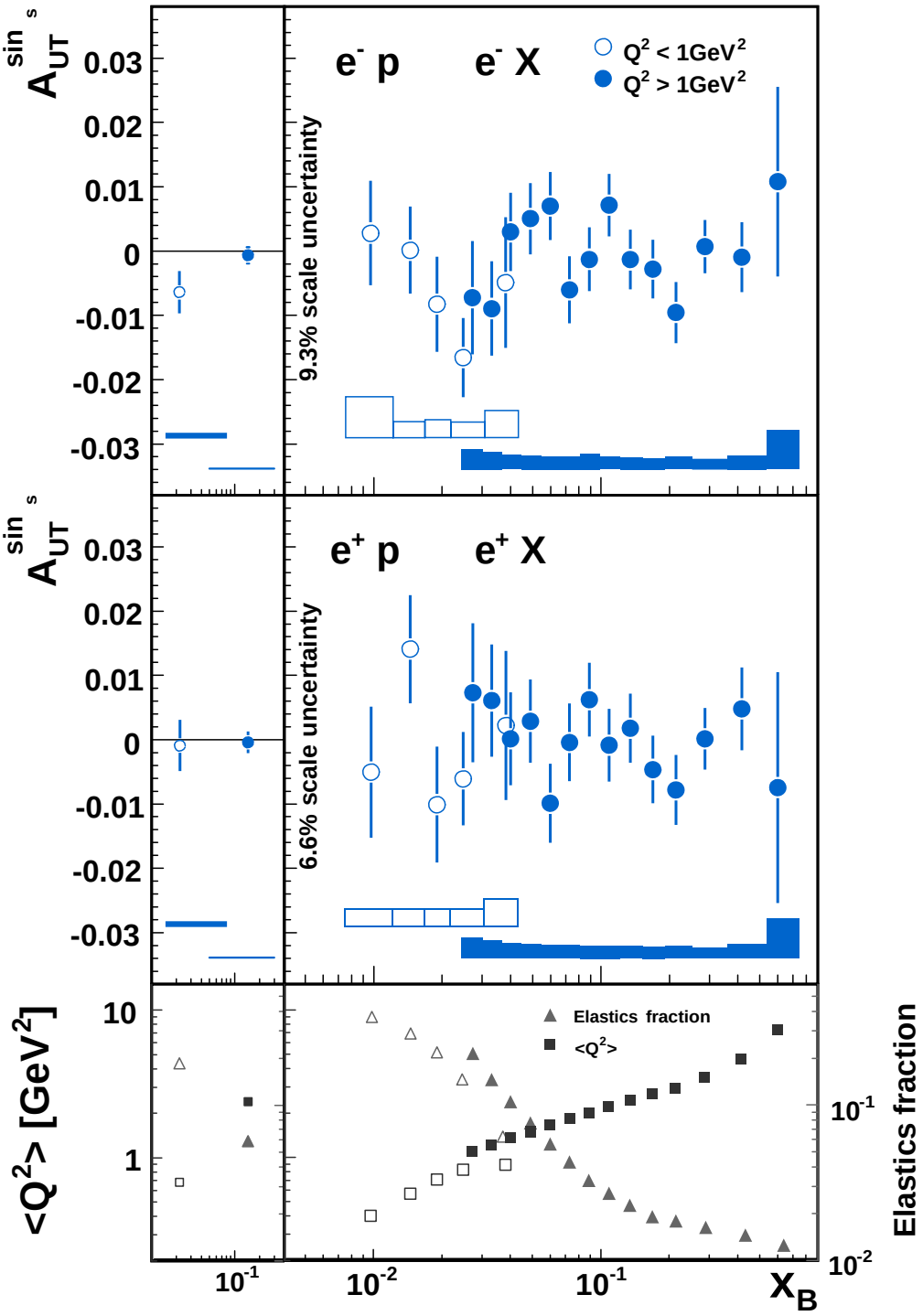

Figure 2b.1: The x_B dependence of the $\sin\varphi_S$ amplitudes $A_{UT}^{\sin\varphi_S}$ measured with an electron beam (top) and a positron beam (center). The open (closed) circles identify the data with $Q^2 < 1$ GeV^2 ($Q^2 > 1$ GeV^2). The error bars show the statistical uncertainties, while the error boxes show the systematic uncertainties. The asymmetries integrated over x_B are shown on the left. Bottom panel: average Q^2 vs. x_B from data (squares), and the fraction of elastic background events to the total event sample from a Monte Carlo simulation (triangles).

2.c Observation of spectator protons in Deep-Inelastic Scattering

A. Martinez de la Ossa (University of Colorado)

Introduction In deep-inelastic electron scattering the quark structure of nucleons is probed. The results are expressed in terms of the structure function $F_2(x)$, which - in the quark-parton model - gives the momentum distribution of quarks in the nucleon x being the Bjorken scaling variable. When a nucleon is embedded in a nuclear environment (characterized by the atomic number A), its corresponding structure function $F_2^A(x)$ is seen to differ from the deuteron structure function $F_2^D(x)$, which approximately represent the average of the (free) proton and neutron structure functions. At low values of x this difference is attributed to shadowing effects, while for $x > 0.1$ the difference is known as the EMC effect [31]. Although the presence of nuclear effects in Deep-Inelastic Scattering (DIS) was first observed more than 20 years ago, no unambiguous explanation for the origin of the EMC effect is available today [32]. On the other hand, various theoretical models [33] exist that are capable of describing the EMC effect. In order to discriminate between such models, additional data are needed that go beyond the inclusive structure function ratio $F_2^A(x)/F_2^D(x)$, on which our current knowledge of the EMC effect is based. Such additional information can be obtained, for instance, by observing spectator nucleons in lepton DIS on nuclear targets: The momentum of the spectator nucleon can be used as a measure (or *tag*) of the local density at which the DIS structure function is probed [34,35]. It is has been argued that it is favorable to use the ratio $F_2^D(x)/F_2^p(x)$ (with $F_2^p(x)$ the proton structure function) for such studies, as complications related to the less well-known structure of heavy nuclei an final state re-interactions are largely circumvented [36]. Moreover, the observation of spectator protons in DIS experiments on deuterium enables an almost model-independent determination of the neutron structure function [37].

Analysis The first goal of the present work is to explore the possibilities offer by the scatter-ingHermes experiment to measure this kind of tagged structure function, by means of the detection of spectator protons produced in lepton DIS on deuterium. The cross section for the observation of a spectator proton in lepton DIS from a deuterium target is given by [38]

$$\frac{\mathrm{d}^5\sigma}{\mathrm{d}x\,\mathrm{d}Q^2\,\mathrm{d}\vec{p}} = \frac{2\pi\alpha^2}{Q^4}\left[1 + \frac{(1-y)^2}{x}\right] F_{2\ tag}^{n}(x, Q^2, \vec{p}) \cdot n(|\vec{p}|). \qquad (7)$$

In this expression Q^2 represents the four-momentum transfer squared, $\vec{p}$ the three-momentum of the spectator proton, α the fine-structure constant, $y = \nu/E$ the fraction of the beam energy E carried by the virtual photon, $F_{2\ tag}^{n}(x, Q^2, \vec{p})$ the tagged neutron deep-inelastic structure function, and $n(|\vec{p}|)$ the momentum distribution of a nucleon in the deuteron.

In principle, the cross section quoted above can be obtained experimentally provided that the scattered lepton could be also measured in conjunction with the spectator proton. However, in order to disentangle both $n(|\vec{p}|)$ and $F_{2\ tag}^{n}(x, Q^2, \vec{p})$ from Eq. 7, is necessary to better obtain the ratio $F_{2\ tag}^{n}/F_2^p$. Thus, the cross section in Eq. 7 needs to be compared to the cross section for inclusive lepton DIS on hydrogen:

$$\frac{d^2\sigma_{DIS}}{dx\, dQ^2} = \frac{2\pi\alpha^2}{Q^4}\frac{1 + (1 - y)^2}{x} F_2^p(x, Q^2) = \frac{N_{incl}^p(x, Q^2)}{\mathcal{L}_{incl} V(x, Q^2)}. \tag{8}$$

where the right-hand side expresses the DIS cross section in measurable quantities. In this expression $N_{incl}^p(x, Q^2)$ represents the yield of inclusive DIS events. $\mathcal{L}_{incl}$ represents the integrated luminosity, and $V(x, Q^2)$ the acceptance in x and Q^2 of the scatteringHermes spectrometer.

The approach approved for the present project to experimentally access the spectator proton momentum distribution $n(|\vec{p}|)$ and the structure function ratio $F_{2\ tag}^{n}(x, Q^2, \vec{p})$ is based on a previous study carried out by scatteringHermes collaboration [39]. That study used DIS data obtained in 1998, when the scatteringHermes experimental setup counted on a Silicon Test Counter (STC) just downstream the target region. It consisted of two layers of double-sided silicon and was positioned beneath the center of the internal target-cell inside the vacuum chamber, in such a way it could be used to observe recoil protons produced in DIS. The present situation is even more favorable and scatteringHermes count on a special recoil detector (RD) surrounding the target region, which makes capable the detection of recoil protons within a larger acceptance. Nevertheless, both experimental configurations are conceptually identical in the sense that involve the measurement of the scattered lepton (using scatteringHermes spectrometer) from DIS on hydrogen and deuterium together with the recoil proton in the recoil detector (RD). Take into account that the spectator protons are exclusively measured with this RD, Eq. 7 can be also rewritten in terms of measurable quantities:

$$\frac{d^5\sigma}{dx\, dQ^2\, d\vec{p}} = \frac{N_{RD}^d(x, Q^2, \vec{p})}{\mathcal{L}_{RD} V(x, Q^2) V_{RD}(\vec{p})}. \tag{9}$$

where $N_{RD}^d(x, Q^2, \vec{p})$ represents the yield of DIS events with an additional proton observed in the RD, and the factor $V_{RD}(\vec{p})$ represents its acceptance of the RD. Combining the last two equations yields:

$$F_{2\ tag}^{n}(x, Q^2, \vec{p}) \cdot n(|\vec{p}|) = \frac{N_{RD}^d(x, Q^2, \vec{p})/\mathcal{L}_{RD}}{N_{incl}^p(x, Q^2)/\mathcal{L}_{incl}} \cdot \frac{1}{V_{RD}(\vec{p})} F_2^p(x, Q^2). \tag{10}$$

With this last equation it is possible to extract either $n(|\vec{p}|)$ or $F_{2\ tag}^{n}/F_2^p$ from the data. The nucleon momentum distribution can be obtained by integrating over x and Q^2, if it is assumed that the total partonic number density is the same for the tagged and untagged structure function. It is seen that the absolute value of the nucleon momentum distribution in deuterium can be derived from the normalized yield for inclusive scattering and the normalized yield of the RD. As the luminosity enters twice it is sufficient to use relative measures of the luminosity as long as the same instrument is used for both.

Spectator proton momentum distribution In order to access to the momentum distributions of spectator protons, the spectrum of recoil protons from DIS on hydrogen and deuterium need to be measured. The hydrogen distribution mainly consists of target fragmentation products from DIS, since spectator protons cannot be produced on hydrogen. The deuterium distribution also contains the sought-after spectator protons. To finally obtain the pure spectator proton momentum distribution we have to subtract the momentum distribution of the fragmentation products as measured on the proton target from the deuterium distribution, assuming the large-angle fragmentation spectra for deuterium and hydrogen to be the same. In doing so, the distributions are normalized using the measured integrated luminosity on each target. This is expressed by the following equation.

$$n(p_{spec}) = \frac{N^d_{RD}(p) - \frac{\mathrm{L}^d_{RD}}{\mathrm{L}^p_{RD}} \cdot N^p_{RD}(p)}{\mathrm{L}^d_{RD} V_{RD}(p)}. \tag{11}$$

with $N^d_{RD}(p)$ and $N^p_{RD}(p)$ the number of proton events in the RD for deuterium and hydrogen targets binned in momentum, L^d_{RD} and L^p_{RD} the integrated luminosity for hydrogen and deuterium for these proton RD events.

Measuring recoil protons in the Recoil Detector In previous section, the motivation and the analysis method for the observation of spectator protons in DIS at scatteringHermes has been presented. It should be clear that the key part of this project consist on the measurement of protons with the recoil detector. Because of that, this section is focus on some technical details of the measurement of low-energetic protons with the new scatteringHermes Recoil Detector.

The scatteringHermes Recoil Detector Since 2006, scatteringHermes counted on a special upgrade: The scatteringHermes Recoil Detector (RD) [40]. This new RD consists of three separate detectors, all surrounded by a superconducting 1 Tesla solenoid magnet. The Silicon Strip Detector (SSD) is the innermost and surrounds the 75µm thickness target cell within the beam vacuum of the HERA ring and inside the scattering chamber. The next detector, outside the scattering chamber, is the Scintillating Fibre Tracker detector (SciFi). The outermost detector is the Photon Detector (PD) which consists of several layers of converter and scintillator material. A schematic drawing of the RD is shown in Fig. 2c.1.

Due to the very low energy of the recoil protons (Fig. 2c.2), it is the inner part of the recoil detector, the SSD, the most important one for this analysis (just a small fraction of recoil spectator protons is expected to reach the outer sub-detectors). For this reason, the design of the recoil detector was thought to minimize the amount of material between the interaction point and the SSD. It is located inside the scattering chamber within the beam vacuum in order to detect those low momentum recoil protons that would otherwise be stopped inside the scattering chamber: only protons with kinetic

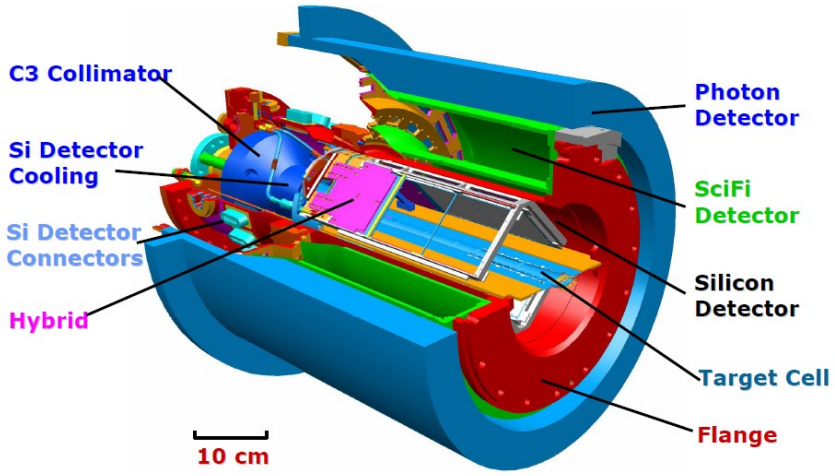

Figure 2c.1: Schematic drawing of the Recoil Detector and its support structure. The Silicon Strip Detector surrounding the target cell is located within the beam vacuum inside the scattering chamber. Continuing outwards are the two concentric barrels of the Scintillating Fibers and finally the Photon Detector. The surrounding superconducting magnet is not shown. The electron beam enters from the left side, where an additional collimator protects the Recoil Detector from synchrotron radiation.

energies of ~14 MeV, corresponding to a momenta of ~160 MeV/c, can pass through the 1.2 mm thickness scattering chamber.

The Silicon Strip Detector (SSD) The SSD consists of eight modules mounted in two layers symmetrically around the target cell in roof-shaped structures (Fig. 2c.3). The two layers are separated by 1.5 cm in which the inner ones are 5.75 cm away from the center of the scattering chamber. The modules are constructed from a ceramic holding frame on which the two silicon sensors are mounted, connected to an aluminum heat sink on which the read-out hybrids are fit. Fig. 2c.4 depicts a schematic view of a module.

On each side of the sensor there are 128 strips with a 758 µm wide pitch. The strip directions of the p-side and the n-side in one sensor are arranged perpendicularly to each other so that two-dimensional position information is available. The electric connection from the detector strips to the hybrids is achieved by 50µm thick polyimide foils (flexleads or flexfoils). The material thickness was minimized so to produce as small a disturbance as possible. The inner modules have their n-side facing towards the cell and p-side facing towards outside, while the outer modules have their n-side facing towards outside and p-side facing towards the cell. This implies that the long flexfoils of the n-side face the target cell and the wall of the scattering chamber, while the short flexfoils on the p-side are between the two module layers. This minimizes the material between the two silicon layers where the particles may have very low momentum.

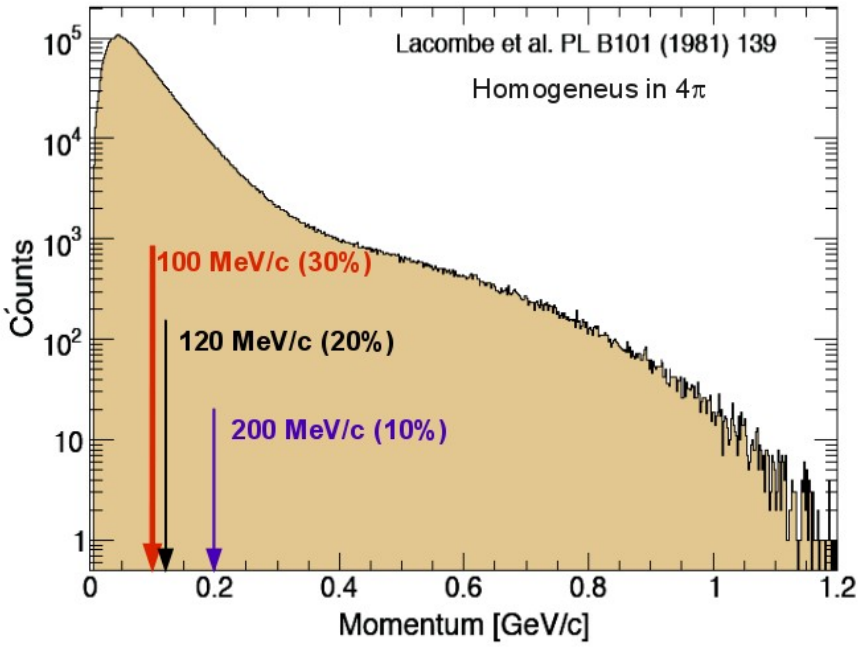

Figure 2c.2: Expected spectrum of spectator protons according with the parametrization of the deuteron wave function done in [41]. Vertical arrows show the minimum reconstructible proton momentum for the case of proton reaching the inner SSD (in red), the outer SSD (in black) and the first SciFi layer (in blue). In percentages, the relative amount of the spectrum which is accessible in each case.

The Scintillating Fibre Tracker detector (SciFi) The Scintillating Fibre Tracker (SFT) is the second detector located after the SSD, going from inside out. The SFT consists of two concentric barrels (with an inner diameter of 109 mm and 183 mm of the inner and outer layer respectively) of 1 mm diameter scintillating fibres, each with a thickness of 4 mm and a length of 280 mm. Each barrel consists of two layers: the fibres of the inner layer are aligned parallel to the beam, while the fibres of the outer layer (stereo layer) are inclined by 10° . This configuration allows the determination of a space point of a particle track for each barrel.

More technical details about SSD and the other recoil sub-detectors can be found in [40].

Reconstruction of low energy protons For any charged track crossing the two layers of SSD modules (inner and outer), the SSD provides two three-dimensional hits or space points (SP) together with the energy deposited by the track in the sensors. This information is used by the standard Recoil tracking system (XTC) to reconstruct the track trajectory and its particle identification (PID). This kind of charged tracks with two SP in SSD can be divided in two main types:

1. Long tracks with hits in SciFi: They are more energetic tracks which go beyond the scattering chamber. Being the SciFi disposed in two parallel layers, it can provide up to two SP more for

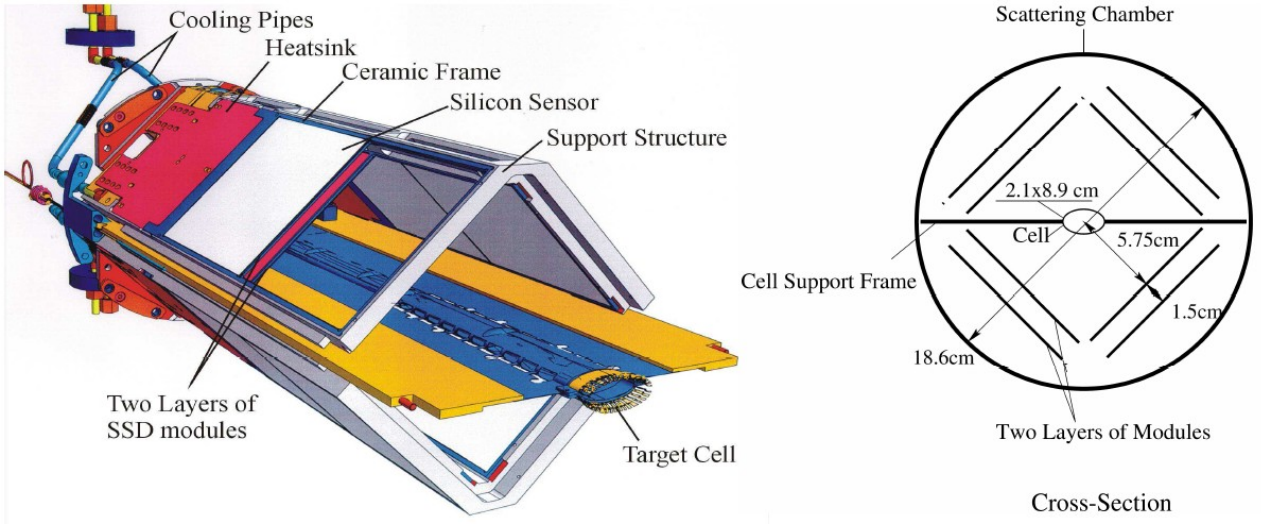

Figure 2c.3: Silicon Strip Detector with the Target Cell. The SSD consists of 8 modules mounted in two layers symmetrically around the target cell. The panel at the right hand side shows the relative position of the SSD in the scattering chamber with the target cell.

a single charged track with their corresponding deposited energy.

2. Short tracks with no hits in SciFi: They are tracks which do not reach the SciFi because of either they were stopped before (in the outer SSD or in the scattering chamber walls) or they were out of the SciFi acceptance.

Long tracks (with SP in the SciFi) provide in general a better determination of the helix parameters which rule its trajectory. In addition, they have more sampling points where their energy deposition is measured. This information is processed by XTC to provide a very precise determination of PID and momentum. For this kind of tracks has been already probed that RD can very efficiently distinguish between proton and pions and thus, make the correct PID hypothesis to measure the particle momentum with high accuracy.

As it was said before, the spectator proton spectrum is expected at low energy and thus, most of the protons coming from this source do not reach the SciFi. Spectator protons belong to the short track case (which only leave signal in the SSD). In Fig. 2c.2, the expected spectator spectrum is shown together with the minimum momentum needed for a proton originated at the target cell to reach the inner SSD (in red), the outer SSD (in black) or the first SciFi layer (in blue). In order to increase as much as possible the momentum acceptance of protons, tracks with only one SP in inner SSD are going to be also consider in the spectator analysis. This set the minimum reconstructible proton momentum to 100 MeV/c.

In spite of most spectator protons give only signal in SSD, this sub-detector is itself an excellent device to measure these low energy protons. Fig. 2c.5 shows the energy deposition of charge par-

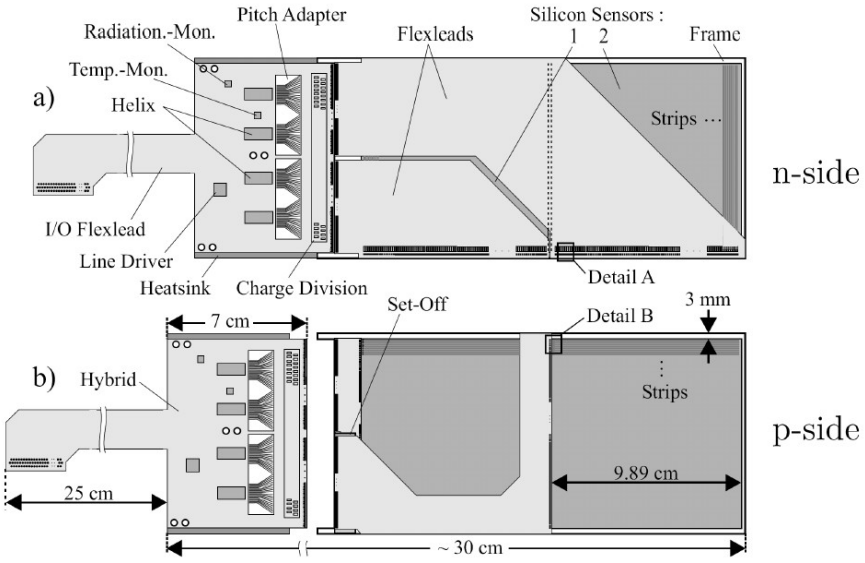

Figure 2c.4: n-side (a) and p-side (b) of a SSD Module. It mainly consists of two double-sided silicon sensors (right side) and two hybrids with the read-out electronics (left side).

ticles in inner SSD (left) and outer SSD (right) as a function of particle momentum. The different energy deposition behavior for protons and pions in the silicon is the base of an efficient PID using just the SSD information.

Tracking efficiency and resolution In order to study the tracking efficiency and the energy resolution of the SSD for low energy protons, a realistic scatteringGeant [30] based simulation of the RD has been done. Protons ranging from 80 MeV/c to 250 MeV/c in momentum have been generated from the target region, isotropically in azimuthal angle and within the zenithal acceptance of the outer SSD. This sample cover by large the expected kinematics of spectator protons. As mentioned above, low energy protons (up to around 200 MeV/c in momentum) only give signal in SSD (short tracks). From the point of the reconstruction, two kind of low protons tracks have been considered in addition:

1. Protons with one single SP in inner SSD.
2. Protons with two SP in inner and outer SSD.

Two space points tracks Up to now, the recoil tracking system (XTC) can only reconstruct tracks with a minimum of two SP in SSD: XTC needs two SP at least to reconstruct the helix of the proton track and make it compatible with the beam line. This geometrical reconstruction is completed with the energy deposition information to perform a kinematic fitting, which gives back a precise determination of the proton momentum.

T

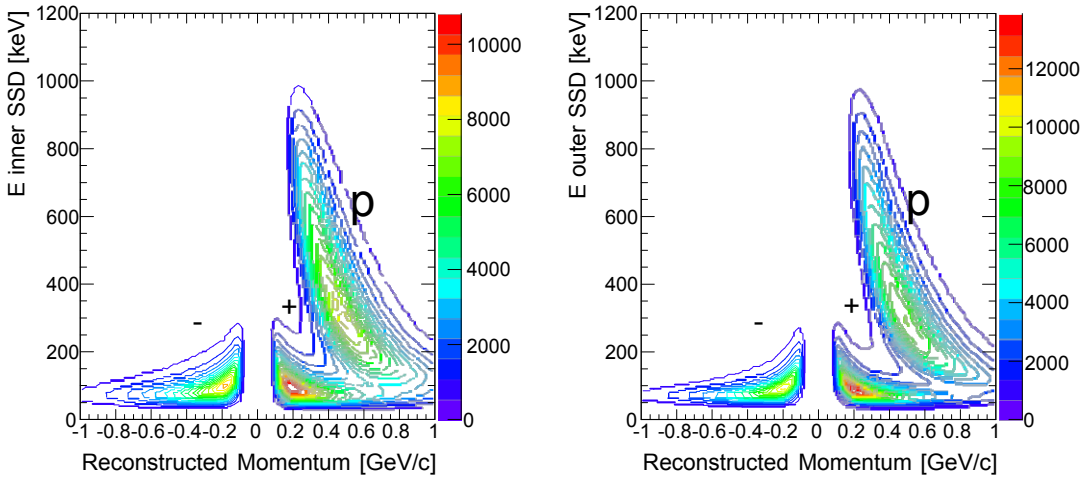

Figure 2c.5: Energy deposition of charged particles in inner SSD (left) and outer SSD (right) as a function of particle momentum. The sign of the momentum represents the charge of the particles.

The ability of XTC to reconstruct a track from a particle which 'actually' hit the inner and outer SSD is called here tracking efficiency. Using this simple one-single-track MC simulation of protons, the tracking efficiency has shown to operate at a superb level (~100%). This value is expected to be a little worse when a more realistic MC scenario with several tracks in the RD is taken into account.

The reconstruction of any track by XTC is always performed under two different hypothesis:

1. The track is a proton: XTC consider that the track is a proton going through inner and outer SSD.

2. The track is a stopped proton: XTC consider that the track is a proton which was stopped in outer SSD.

The use of one or other hypothesis can lead to rather different results. Fig 2c.6 shows the different energy deposition behavior of protons which stop in the outer SSD or go through. Depending on the proton was really stopped or not in the outer SSD, the value of the deposited energy in outer SSD correspond with different momentum (this illustrated with the two branches in lambda shape of Fig. 2c.6). Since there is no way to know a priory if a track with just two SP in SSD was stopped in outer SSD or went through, this two hypothesis are always taken into account in the reconstruction.

In Fig. 2c.7, the difference between reconstructed and generated momentum vs. generated momentum of protons reaching the outer SSD is shown. Proton hypothesis gives a rather optimal resolution when available, while something strange happen with the stopped proton hypothesis: Resolution is not totally wrong, but exhibits some "strange" or erratic regions where the reconstructed

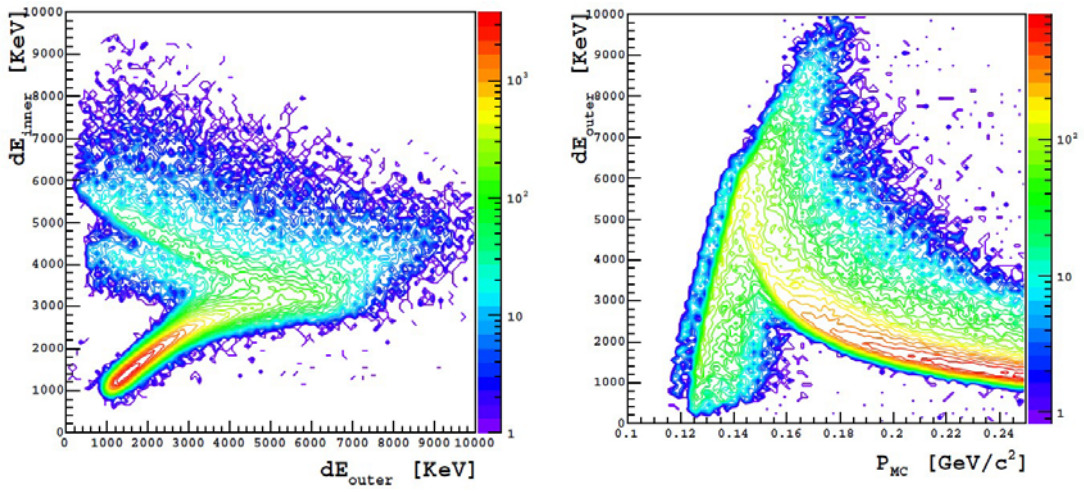

Figure 2c.6: (left) The deposited energy in inner SSD vs. outer SSD of generated protons. (right) The deposited energy in outer SSD vs. the generated proton momentum. The shape of the distributions clearly shows the two branches corresponding to the stopped and through going protons.

momentum deviates from the generated one by more than 20%. In order to figure out the reason of this effect, a special sample of protons has been generated with their starting *z* position fixed at the center of the target region. The generated azimuthal angle φ_{MC} is also restricted to one of the RD quadrants.

From this sample, only the protons with the stopped proton hypothesis available have been consider. In Fig. 2c.8 (left), the difference between reconstructed and generated momentum vs. generated momentum of protons reaching the outer SSD. The "erratic" zones has been marked with different colors. In Fig. 2c.8 (right), the generated azimuthal angle φ_{MC} vs. the generated zenithal angle θ_{MC} of the same sample of protons is also plotted. Being the initial *z* coordinate fixed for these protons, the right plot in Fig. 2c.8 is like a "map" or "image" of the different regions in the SSD sensors (see Fig. 2c.4). The gap between sensors in each SSD module and the contours of the flexfoils for the n-side and p-side of inner SSD and the p-side of the outer SSD, can be perfectly distinguished. Without entering in details, this result address the cause of problem to a wrong passive material correction in the case of stopped proton hypothesis. Clearly, there are protons going through the flexfoil material in SSD which are not corrected by the energy looses. On the other hand, there are protons which did not pass through one of the flexfoil planes which are over corrected. There is also a special region (zone 3 in Fig 2c.8), which is worth to be commented: These are protons with a very large underestimation of their energy (even bigger than 30%). The latter effect is always correlated with large incident angles, or when the energy looses in the walls of the scattering chamber are more significant and/or the momentum of the proton is out of the SciFi acceptance. In this case is easier than a higher energy proton has no chance to deposit energy in the SciFi and the XTC make

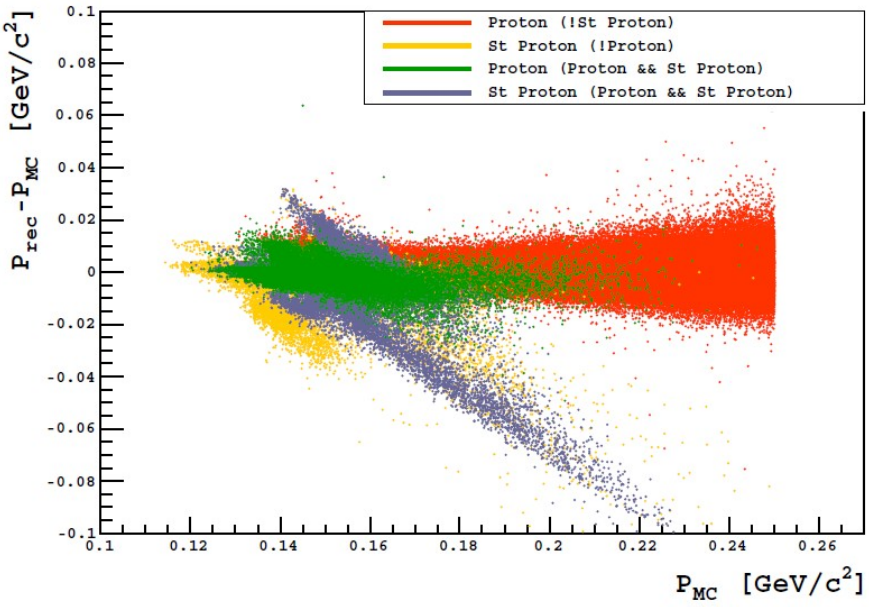

Figure 2c.7: Difference between reconstructed and generated momentum vs. generated momentum of protons reaching the outer SSD. Different colors show different distributions depending on the different hypothesis taken into account: protons reconstructed only under proton hypothesis (red), protons reconstructed under proton hypothesis, but with the stopped proton hypothesis available (green), protons reconstructed under stopped proton hypothesis, but with the proton hypothesis available as well (blue) and protons reconstructed only under stopped proton hypothesis (yellow).

the mistake of consider it as a stopped proton.

These resolution problems are currently being solved by the scatteringHermes collaborators and are expected to be ready in a short term. Hopefully, this will lead to a optimal reconstruction of short protons with two SP in SSD.

One space point tracks About 10% of the accessible spectator proton spectrum (Fig. 2c.2) is expected to fall in the kind of tracks which never reach the outer SSD. Since XTC do not deal with these single hit tracks a special treatment is required. The absolute momentum of the proton can be obtained from the deposited energy in inner SSD. Fig. 2c.9 shows the energy deposition of the protons in the inner SSD. Similarly to the case of two SP protons, there is an ambiguity in the determination of the momentum from the deposited energy as it could correspond to different values of the initial momentum depending on the proton was really stopped in inner SSD or not. Due to that, it is needed to always make the correct *ansatz* for a track with just one SP in the inner SSD. In other words, the reconstruction of one single SP tracks can be done only under the hypothesis that the particle was stopped in the inner SSD sensor. This difficulty can be solved by means of defining a fiducial cut which ensures that the track, in the hypothetical case it would have crossed the inner

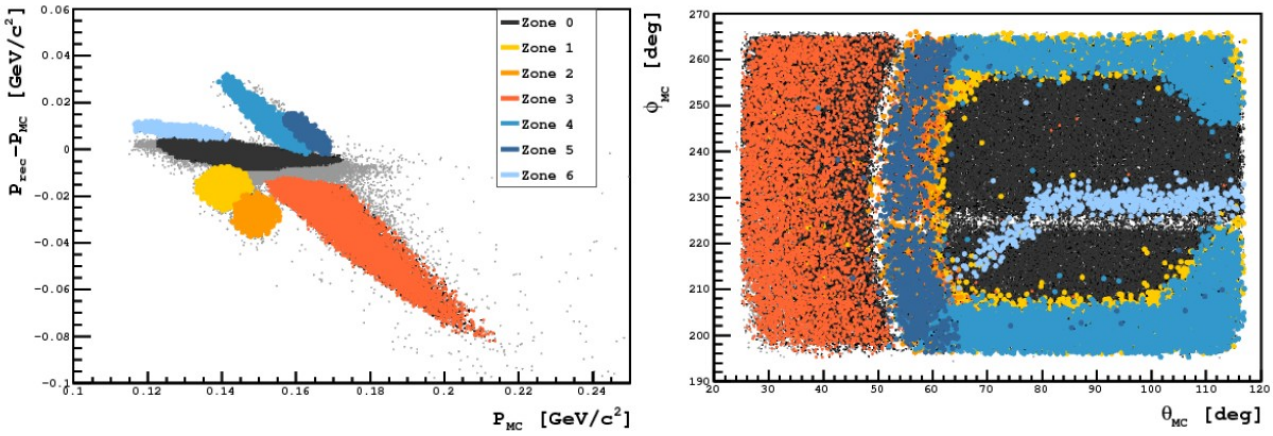

Figure 2c.8: (left) Difference between reconstructed and generated momentum vs. generated momentum of protons reaching the outer SSD and reconstructed only under stopped proton hypothesis. (right) The generated azimuthal angle φ_{MC} vs. the generated zenithal angle θ_{MC} of the same sample of protons. Different zones (indicated by means of colors) in left plot correspond to well determined geometrical zones in SSD sensors.

SSD, would reach the outer SSD. The idea is to use the outer SSD as a veto for through going tracks. The latter implies to properly define a fiducial volume, which takes into account the details of the outer SSD geometry.

The last piece of the puzzle still remains: How to measure the direction of these single SP protons? Clearly, only with one SP and the beam constrain is not enough to completely determine the direction of a track (the zenithal angle θ would remain undetermined). Nevertheless, since the analysis of tagged structure function require to measure spectator proton in conjunction with the scattered lepton, is always possible to take the *z* position of the main interaction vertex from the reconstruction of the lepton.

Conclusion The analysis of spectator protons (or tagged structure functions) in DIS at scatteringHermes has been outlined in this document (Sec. 2.c). Although the project still being in a development stage, preliminary studies show that it will be possible to access about the 30% of the spectator proton spectrum using the new Recoil Detector installed in scatteringHermes for the last two years of data taking. First results are foreseen by the end of the year.

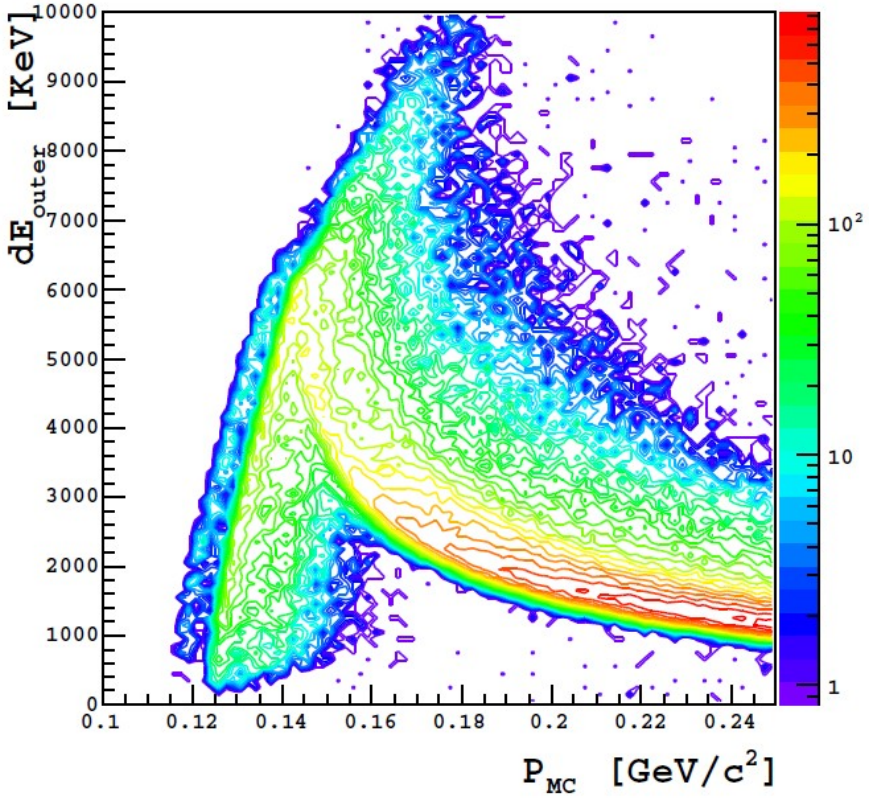

Figure 2c.9: The deposited energy in inner SSD vs. the generated proton momentum. The left branch of the distribution correspond to the protons stopped in inner SSD.

References

[1] C. E. Hyde and K. de Jager, Ann. Rev. Nucl. Part. Sci. **54**, 217 (2004).

[2] P. A. M. Guichon and M. Vanderhaeghen, Phys. Rev. Lett. **91**, 142303 (2003).

[3] P. G. Blunden, W. Melnitchouk, and J. A. Tjon, Phys. Rev. Lett. **91**, 142304 (2003).

[4] J. Arrington, W. Melnitchouk, and J. Tjon, Phys. Rev. **C76**, 035205 (2007).

[5] A. V. Afanasev and C. E. Carlson, Phys. Rev. Lett. **94**, 212301 (2005).

[6] J. Mar *et al.*, Phys. Rev. Lett. **21**, 482 (1968).

[7] A. Metz, M. Schlegel, and K. Goeke, Phys. Lett. **B643**, 319 (2006).

[8] J. Arrington, Phys. Rev. C **69**, 032201 (2004).

[9] scatteringSample Collaboration, S. P. Wells *et al.*, Phys. Rev. **C63**, 064001 (2001).

[10] scatteringA4 Collaboration, F. E. Maas *et al.*, Phys. Rev. Lett. **94**, 082001 (2005).

[11] scatteringG0 Collaboration, D. S. Armstrong *et al.*, Phys. Rev. Lett. **99**, 092301 (2007).

[12] H. Jostlein *et al.*, Phys. Lett. **B52**, 485 (1974).

[13] S. Hartwig *et al.*, Lett. Nuovo Cim. **15**, 429 (1976). [14]

D. L. Fancher *et al.*, Phys. Rev. Lett. **37**, 1323 (1976). [15]

L. S. Rochester *et al.*, Phys. Rev. Lett. **36**, 1284 (1976). [16]

S. Hartwig *et al.*, Phys. Lett. **B82**, 297 (1979).

[17] scatteringEmc, J. J. Aubert *et al.*, Nucl. Phys. **B272**, 158 (1986).

[18] scatteringBcdms Collaboration, A. Argento *et al.*, Phys. Lett. **B140**, 142 (1984).

[19] J. A. Appel *et al.*, Phys. Rev. **D1**, 1285 (1970).

[20] J. R. Chen *et al.*, Phys. Rev. Lett. **21**, 1279 (1968).

[21] S. Rock *et al.*, Phys. Rev. Lett. **24**, 748 (1970).

[22] N. Christ and T. D. Lee, Phys. Rev. **143**, 1310 (1966).

[23] A. Afanasev, M. Strikman, and C. Weiss, Phys. Rev. **D77**, 014028 (2008).

[24] X. Jiang *et al.*, Jefferson Lab Hall A Experiment E-07-013 (2007).

[25] scatteringHermes Collaboration, K. Ackerstaff *et al.*, Nucl. Instrum. Meth. **A417**, 230 (1998).

[26] A. Nass *et al.*, Nucl. Instrum. Meth. **A505**, 633 (2003).

[27] scatteringHermes Collaboration, A. Airapetian *et al.*, Nucl. Instrum. Meth. **A540**, 68 (2005).

[28] G. Ingelman, A. Edin, and J. Rathsman, Comp. Phys. Commun. **101**, 108 (1997).

[29] I. Akushevich, H. Boettcher, and D. Ryckbosch, (1999), hep-ph/9906408.

[30] R. Brun, R. Hagelberg, M. Hansroul, and J. Lassalle, scatteringCern Report scatteringCern-DD-78-2-REV (1978).

[31] European Muon, J. J. Aubert *et al.*, Phys. Lett. **B123**, 275 (1983).

[32] G. A. Miller and J. R. Smith, Phys. Rev. **C65**, 015211 (2002), nucl-th/0107026.

[33] P. R. Norton, Rept. Prog. Phys. **66**, 1253 (2003).

[34] L. L. Frankfurt and M. I. Strikman, Phys. Rept. **160**, 235 (1988).

[35] C. Ciofi degli Atti and S. Simula, Phys. Lett. **B319**, 23 (1993).

[36] W. Melnitchouk, M. Sargsian, and M. I. Strikman, Z. Phys. **A359**, 99 (1997), nucl-th/9609048.

[37] S. Simula, Phys. Lett. **B387**, 245 (1996), nucl-th/9605024.

[38] S. Simula, Nucl. Phys. **A631**, 602c (1998).

[39] J. Visser, DESY-HERMES-02-47.

[40] HERMES-Collaboration, HERMES Internal Note 02-003 (2001).

[41] M. Lacombe *et al.*, Phys. Lett. **B101**, 139 (1981).

3. The Fermilab Seaquest (E906) Experiment

E.R. Kinney, J. Katich, P.-J. Lin (University of Colorado), The Seaquest (E906) Experiment

The Seaquest collaboration at Fermilab (E906) [1] will extend measurements of the light quark sea to significantly higher x using DY reactions of 120 GeV/c protons with nucleon and nuclear targets. In the DY process, a quark (or antiquark) in the beam (with momentum fraction x_1) annihilates with an antiquark (quark) in the target (with momentum fraction x_2). At large rapidity (large $x_F \approx x_1 - x_2$) the reaction is dominated by annhiliation of a beam quark with a (fixed) target antiquark, hence one is able to probe the antiquark sea of the target hadron. The advantage over earlier Fermilab DY experiments is the lower beam energy, since the cross section scales as $1/E_{beam}$ for fixed Bjorken x. This will allow us to determine the light sea quark distribution up to higher x than in previous measurements, allowing more stringent tests of models and perhaps an explanation for the "low" value of the Gottfried sum.

The primary goal of the experiment is the precise determination of the light sea ratio, $\bar{d}(x_2)/\bar{u}(x_2)$, with a 1% systematic uncertainty, using the ratio of cross sections in pd and pp collisions. In addition Drell-Yan *absolute* cross sections from p and d will be measured with absolute normalization uncertainty of 6.5% in the range of $0.3 < x_1 < 0.9$ and $0.05 < x_2 < 0.5$. Projections for the statistical accuracy of the light sea are shown in the left panel of Fig. 3.1 compared to earlier measurements and the prediction from the CTEQ6 [2] quark distributions. It should be noted that no physical models at present are able to explain the drop in the ratio below 1 at high x, already observed in E866 [3]. In addition to the light sea ratio, these cross section will provide a strong constraint on the high x quark distributions.

Drell-Yan cross sections from nuclear targets, such as C, Ca, Fe, and W, will also be determined. These data will allow the comparison of the sea quark distribution in nuclei to that in the deuteron. Earlier measurements [4] of Drell-Yan in nuclei (Fermilab E772) saw essentially no significant modification of the nuclear cross section dependence on x_2 above 0.1, in contrast to that observed in deep inelastic scattering, originally by the EMC [6], and more thoroughly by later experiments [7–9]. The right panel of Fig. 3.1 shows the statistical precision that is expected from the Seaquest measurement of the ratio of Ca to ^{2}H, compared to earlier deep inelastic experiments as well as the Drell-Yan measurement of E772. These data will be able to resolve the question of whether an anti-shadowing region exists in the Drell-Yan ratio, and moreover at the highest x, whether the so-called "EMC" effect around $x \sim 0.5$ is also seen by the Drell-Yan process. In addition to the nuclear sea ratio, the measurements on nuclear targets at high x_1 can strongly constrain models of fast quark energy loss in "cold" nuclear matter. The energy loss of a colored quark in the nucleus is not only a basic QCD process; its understanding is critical to the interpretation of results from the recent measurements at

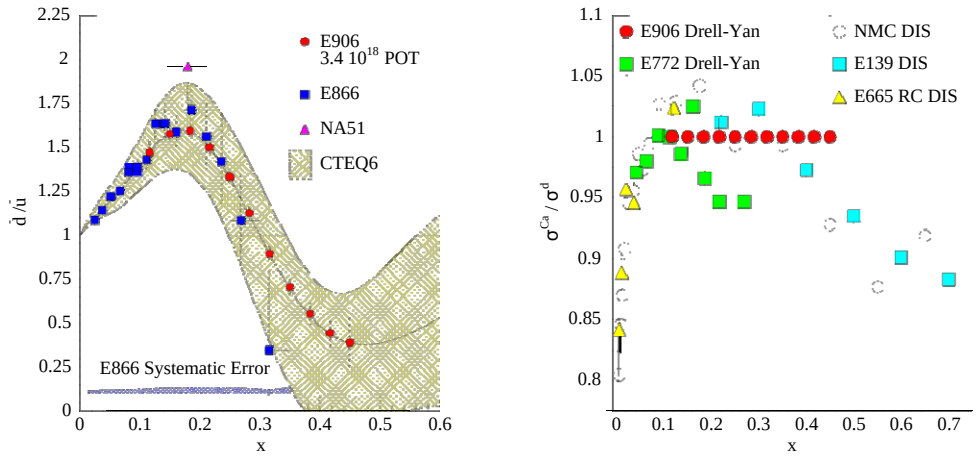

Figure 3.1: Left panel: Projected statistical accuracy of the Seaquest measurement of the light sea ratio $\bar{d}(x_2)/\bar{u}(x_2)$ assuming the CTEQ6 [2] quark distributions and 3.4×10^{18} protons on target. Results from the previous experiments NA51 [5] and E866 [3] are shown for comparison. Right panel: Projected statistical accuracy of the E906 measurement of the ratio of Drell-Yan cross sections of Ca and ^{2}H, compared with the previous experiments [4, 7–9].

the relativistic heavy ion collider.

The determination of these light quark distributions has broad impact, in astrophysics, neutrino physics, and spin physics. One can also use the DY process to study the energy loss of the initial beam quark as it passes through the nucleus before annihilation. Three nuclear targets of different size will be used to vary the average path length. Energy loss is expected to increase significantly at the lower beam energy (as $1/s$) while the higher x of the target antiquark should be further removed from the shadowing region. The lower energy data should also help resolve uncertainty in the interpretation of the earlier 800 GeV/c experiments. We expect these energy loss studies to complement those from our past studies at the HERMES experiment, which are more sensitive to the details of the hadronization of the struck quark.

The original E906 proposal [1] was submitted in 1999; a revised proposal was given stage II approval by the Fermilab PAC in 2005, however running was deferred many years until a match between available DOE funding and a redesigned di-muon spectrometer was achieved. Assembly of the spectrometer began in earnest in 2009 in the NM4 hall at Fermilab, however, a number of technical difficulties with the spectrometer and with the beamline have resulted in significant delays. In fact, first physics running has started in spring 2014. Figure 3.2 shows a perspective view of the spectrometer. To keep costs low the collaboration has assembled the spectrometer using many components from the previous E866 experiment. The actual design is very similar to that of E866, comprising a solid iron focusing dipole magnet containing the beam dump, followed by a large open aperture dipole for precise momentum determination. Multi-wire proportional and drift chambers

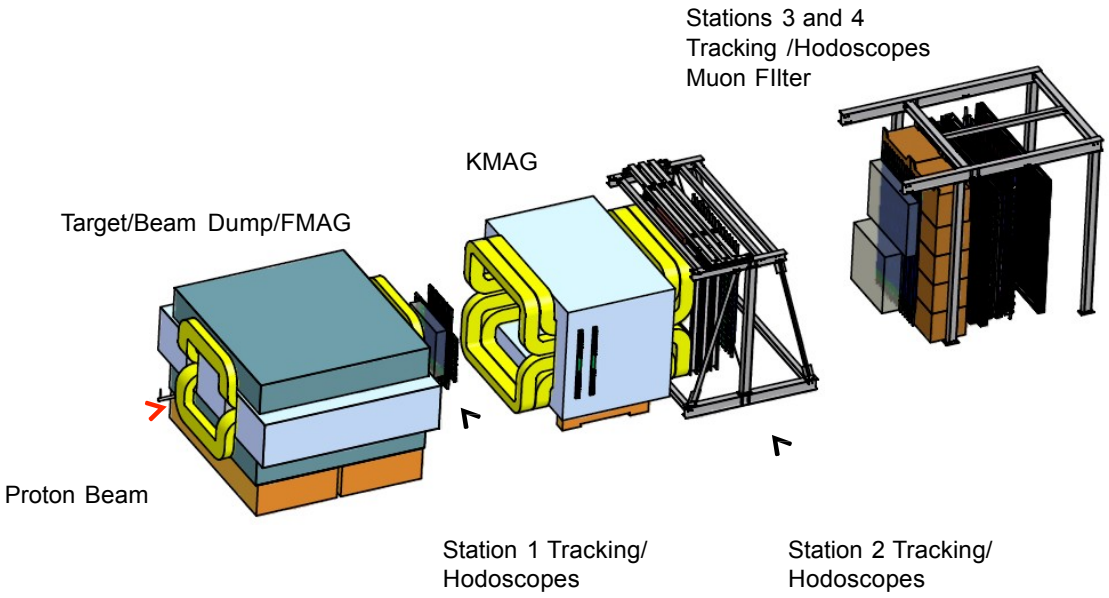

Figure 3.2: Perspective View of E906 Di-muon Spectrometer.

between the first two magnets as well as after the second dipole provide tracking information, supplemented by scintillation hodoscopes used primarily for fast triggering. A final large iron absorber instrumented with proportional tubes provides muon identification.

References

[1] http://www.phy.anl.gov/mep/SeaQuest/index.html .

[2] J. Pumplin, D.R. Stump, J. Huston, H.L. Lai, P.M. Nadolsky and W.K. Tung, JHEP **0207**, 012 (2002).

[3] R.S. Towell *et al., Phys. Rev.* **D64**, 052002 (2001).

[4] D.M. Alde *et al., Phys. Rev. Lett.* **64**, 2479 (1990).

[5] A. Baldit *et al., Phys. Lett.* **B332**, 244 (1994).

[6] J.J. Aubert *et al., Phys. Lett.* **B123**, 275 (1983).

[7] P. Amaudruz *et al., Nucl. Phys.* **B441**, 3 (1995).

[8] M.R. Adams *et al., Z. Phys.* **C67**, 430 (1995).

[9] J. Gomez *et al., Phys. Rev.* **D49**, 4348 (1994).

3.a Status of Station 1 Tracking Chamber

At the time of 2005 proposal, the Colorado group has taken responsibility for construction of front tracking chambers (MWPCs) as its hardware commitment to the experiment. These chambers will be located just after the target/beam dump magnet and so see a high rate of charged particles. No existing suitable chamber with sufficient granularity and size was available. Plans were made to use the Fermilab wire chamber shop to perform the wire stringing on one of the existing winding tables. When the spectrometer was redesigned after 2005, monte carlo studies indicated that to fully take advantage of the new spectrometer acceptance, the chambers needed to be larger than originally planned. The new larger size could not be handled by the existing Fermilab winding apparatus, and furthermore, was now of a size that the originially planned use of cathode foils was problematic, from both mechanical and electrical stability issues.

A new design was developed based on the use of precision milled endplates with crimped pins to hold the individual wires (both cathode and anode planes are now wire planes), similar to that used in the tracking chambers provided by the Seaquest Japanese collaborators. A prototype was built and it was quickly determined that crimped pins were not feasible. Following an idea developed for SSC tracking chambers, we developed a design where each end of the wires was threaded through small plastic sleeves which fit into the machined holes. After the wire was strung through these holes, a metal pin was inserted and glued in place to both establish electrical contact for connection to the chamber electronics as well as mechanically hold the wires in place. This design was tested and refined using our prototype chamber. Finally, the full wire frame and machined endplates were fabricated and the stringing of the roughly 8000 wires began in June 2013, performed by Katich, Lin, and undergraduate Brian McDonald, and was completed in February 2014.

C. FUNDAMENTAL NUCLEAR SYSTEMS AND INTERACTIONS

1. Main Injector Particle Production - FermiLab E907

R.J. Peterson (University of Colorado) and the MIPP Collaboration

Our first spell of beam for this experiment was completed in 2007, and analysis of the runs has been carried out to the stage where some results are ready for publication. Our experiment generated mixed but tagged beams of pions, kaons and nucleons, of both signs, from the 120 GeV proton beam of the Fermilab Main Injector, incident of a copper production target. These secondary beams were incident upon thin samples of complex nuclei, with the reaction products analyzed by a string of detectors able to cover a very wide range of outgoing energies and species. Prof. Peterson is the target czar, and was responsible for the array of thin samples. We have completed scans of several targets at one or two energies, and scans of a few targets across a wider range of energies, from xx to yy GeV. We have used the Time Projection Chamber, the first device after our reaction targets, to measure the mean multiplicities of particles on samples of Be, C, Cu, Bi and U at 58 Gev. Our analysis included ejectiles with momenta from 0.12 to 1 GeV/c. With six beam species and six reaction products, on five nuclei, we have the beginning of a data set well-suited to studies of hadron propagation within nuclei. Final mean multiplicities will be available by October, with the analysis lead by the group newly formed at Wichita State University. Also, a draft of a NIM paper using the RICH detector at the end of our string of detectors to measure the K+ mass is in circulation. In addition to our thin samples, E907 also put the 120 GeV proton beam onto a clone of the NuMI neutrino-source target, to understand the number of pions and kaons produced. The decay of these ejectiles is the source term for NuMI neutrinos, and is the least understood feature of that large project. Results have been summarized in PhD theses at Harvard. Meanwhile, significant improvements to our detector systems have been carried out, such that future data rates can be much higher, enabling us to pursue more complete studies of the target mass and beam species/energy dependence of many observables. We also expect to be able to use lower momentum beams. We will be invited to present our proposal for more beam time to the Fermilab PAC soon after we demonstrate our work in print, perhaps in the fall of 2009.

2. Scaling Relations among Intermediate Energy Hadron Spectra

R.J. Peterson (University of Colorado)

It has been observed that the continuum spectra of electrons scattered from complex nuclei can be arranged by kinematic transformations to yield generally comparable responses, by mechanisms

known in general as scaling. One makes some assumption about the scattering, based upon one and only one elastic and incoherent interaction of the electron with individual bound nucleons. Quite an industry has arisen to use these quasifree (called quasielastic in the electron community) responses to understand the internal momentum dynamics of complex nuclei. Similar kinematic conditions can be attained with hadron beams, and there is a useful array of relevant continuum data, using beams of proton and mesons, with both scattering (non charge exchange or NCX) and single charge exchange (SCX) spectra. These hadron beams do not have the weak and simple attributes of electron scattering, but it was deemed useful to see to what extent hadron continuum spectra exhibit scaling phenomena similar to what is seen with electrons. With the same basic assumption of one and only one incoherent scattering, we can use scaling, if observed from the data, to draw inferences about hadronic interactions within the nuclear medium. We can also use spin and isospin variables offered by hadrons to infer the full array of spin and isospin responses of nuclei. Electrons access but two of the six possible responses. It was necessary to develop means to deal with hadronic complications. First, how many one-an-only-one collisions might there be? The Glauber model was developed and applied to count these. [Ouyang, PRC47 2809] This model requires inputs of the distribution of nucleons, and we developed an unfolding system to determine these distributions from measured distributions of nuclear charge. [Patterson NPA 717, 235] Also in the calculation is the in-medium hadron-nucleon total cross section. We adjusted this to seek agreement with the target mass dependence of y-scaling responses. [RJP NPA740, 119] The role of nuclear binding is different for hadrons than for electrons, especially in SCX, where the Coulomb energy enters with some sensitivity. This was shown by comparing the quasifree maxima for both pion beam charges in SCX reactions. [RJP PLB 297, 238] We even carried out the difficult study of quasifree K+ scattering, in order to use this most penetrating of hadronic beams. [Kormanyos PRC 51, 669] We also examined the complete range of nuclear spin observables in the isoscalar channel by quasifree deuteron scattering, although the theoretical methods were not able to allow the presentation of actual nuclear responses [Holcomb PRC 57, 1778] A series of papers used the y-scaling scheme, the one most commonly used with electrons, for both NCX and SCX hadron reactions. Only one of the published hadron studies was designed to test scaling ideas [Fujii PRC 64, 034608], and was so analyzed. [RJP PRC65, 054601] A probably-complete array of relevant hadron data was used in two papers, for NCX [RJP NPA769, 390] and for SCX reactions [RJP NPA 769, 115]. Although it would seem intuitive that higher hadron beam energies would give cleaner kinematic responses, as found with electrons, in fact the lab frame hadron differential cross sections at energies significantly above 1 GeV are so strong and so forward peaked that a given momentum transfer is more readily attained in several steps, violating the scaling condition. These papers were able to map out both the lower and upper beam energy ranges suited to scaling analysis, as well as the angle or momentum transfer limits, before more complex mechanisms blur the simple responses. Scaling is more reli-

ably followed for lighter nuclei. Recent electron work was able to use the alternative Bjorken scaling system to demonstrate the effect of Short range Corrleations (SRC) in continuum spectra [Egiyan PRC 68, 014313] This effort was mirrored in analyses of hadron NCX [RJP NPA 791,84] and SCX [RJP NPA 803,46] responses, which demonstrated much the same behavior as noted with electrons. The responses of heavier nuclei show greater strength at xB¿1 or 2 or 3 than noted for light nuclei. Our work extended the results to the explicitly isovector channels, using SCX. During the AGS runs with the Crystal Ball detector, we were able to obtain pion SCX cross sections across a very wide angle range on C, Al and Cu targets. At the special momentum of 750 MeV/c, it so happens that the nonspin and (transverse) spin amplitudes for pion SCX vary strongly with angle. We showed how an analysis similar to the familiar Rosenbluth decomposition with electrons could be used to separate the spin and nonspin isovector responses from these data. If the ratio of these simply tracked with angle, it would be hard to believe that kinematic and spin effects could be separated, but since the ratio of these cross sections goes up, down, up, and down again with angle, one can trust the spin analysis. We showed that the isovector transverse spin responses of our samples agreed with results from electron scattering, as a test. We then provide a new response, the isovector nonspin response of these nuclei. [RJP PRC 69, 064612] Large IntraNuclear Cascade (INC) codes are used to model the reactions of intermediate energy protons in thick targets, for instance for neutron spallation sources. These codes do not do well at reproducing the very highest energy outgoing products, which are important for shielding designs and for the continuation of cascades in thick samples. These are just the energy ranges examined by scaling methods, and the observed scaling have been used to systematize the spectra for (p,px) and (p,nx) reactions, especially on heavy elements. The few experiments are thus able to be compared, an especially valuable means to evaluate and interpolate and possibly extrapolate the very hard and scarce measurements of the highest energy neutrons. This has been completed, and reported in a form suited to be used by spallation source designers. [RJP NSE 161, 346] This extensive program, including technical developments of the method, experimental observations, and two scaling techniques, is now complete and published, with fairly good representation at relevant conferences.

3. Local potentials for pion-nucleus scattering

R.J. Peterson (University of Colorado)

Proton-induced reactions induced in nuclei, either in thin samples or in thicker targets such as used for neutron spallation sources, will involve the production, transport, and absorption of pions. Transport codes use optical model formulations to assist these calculations. The pions, however, with their fundamentally resonant interactions with nucleons, encounter nuclear potentials with complications. For instance, across the delta region, the interaction is driven largely by a noncentral p-wave

interaction, usually dealt with by a special DWIA code, much different from those local codes used for baryons. Satchler derived and demonstrated a means to transform the relevant nonlocal Klein-Gordon equation for pions into a local potential, such as used for baryons. A transformation of the mass and beam energy is involved. [1] Excellent fits to a sample of elastic scattering data were obtained. However, an ambiguity arises due to the very strong absorption of pions, especially at the delta region. In collaboration with a patient group in Bangladesh, we found that also insisting that the fitted potential parameters give the correct shape and magnitude of collective inelastic pion scattering resolved this ambiguity. [2] Essentially, we were determining the potential and its first derivative by this joint fitting. The Bangladesh group has extended this fitting, with the inelastic constraint, to essentially all published pion-nucleus elastic scattering data, from carbon through lead, at energies from 100 to 2000 MeV. The publication of this work has been retarded by poor communications, retirements, and illness in Dhaka, but we did prepare and present our work at a conference with the users of Fluka. [3] We found a systematic set of geometrical parameters for the 3-parameter Woods-Saxon real and imaginary local potentials, and the well depths found by the fitting showed a strong resonant behavior, seen in Figures X-1 and X-2. These trends have been fitted to the simple single-resonance-plus-hard-sphere equations for scattering amplitudes. This project is essentially complete, although it is hoped to extend the fitting effort to data at pion kinetic energies below 100 MeV. A paper, complete except for such cases, is complete, and awaiting approval and final wording by all authors. When presented, a great simplification will be possible for those who create and use complex transport codes, since only a single optical model formulation will also be able to include pion reactions. In addition, detailed trends, especially at resonance energies, of the potential depths for both pion signs on samples with a range of neutron excesses are noted. The figures do not distinguish these cases, since this presentation emphasizes the general trends of the potential families, but the isospin sensitivities are the source of the scatter in data points at fixed energies. These features are treated in detail in our complete paper.

References

[1] G.R. Satchler, Nucl. Phys. A **540**, 533 (1992).

[2] Md.A.E. Akhter *et al.,* Jour. Phys. G **27**, 755 (2001).

[3] D.R. Sarker *et al.,* Proc. 2009 Varenna Conference on Nuclear Reaction Mechanisms.

4. Nuclear Astrophysics

R.J. Peterson (University of Colorado), N. Burtebaev (Institute of Nuclear Physics, Republic of Kazakhstan, Almaty), R. Yarmukhamedov (Institute of Nuclear Physics, Republic of Uzbekistan,

Tashkent)

Our large paper on the $^{12}C(p,\gamma)^{13}N$ reaction has appeared in Phys. Rev. C [1]. This work includes new measurements of the gamma ray yields from low energy proton beams provided by an accelerator in Almaty, Kazakhstan, and a very thorough theoretical analysis, carried out in Tashkent, Uzbekistan. Proton stripping spectroscopic factors, as reported last year, enter this analysis. Interestingly, the results of our new work agree more closely with the thick-target results obtained years ago with our Boulder cyclotron [2] than with other, more recent, measurements.

Our Boulder thick-target method has many advantages, but the results are a bit old. Newer beams, detectors, and dE/dx methods should allow improved results, and our Central Asian collaboration is designing new experiments to bring this method back to life, using the same general ideas as carried out originally and low energy proton beams in Kazakhstan and Turkey.

The same idea, relating yields of reaction products from beams stopping in a thick sample, could also be used in reverse kinematics. For instance, a 6 MeV carbon stopping in a hydrogenated thick target should be equivalent in ^{13}N yield to the use of a 500 keV proton beam into carbon. The Almaty team has mastered the proprietary technology to make thin films of a conducting material rich in hydrogen. We intend to use the new heavy-ion cyclotron in Astana, Kazakhstan to see if the thick target results from reverse kinematics match the more usual yield and thermonuclear reaction rate results.

If this method can be demonstrated, the door is open to the use of thick hydrogenated (or deuterated) samples to measure the reaction rates of secondary beams of short-lived activities. This is likely to be more reliable and more efficient than other methods, and could revolutionize laboratory methods for astrophysically important nuclear reaction rates.

Most of this work is supported by Uzbek, Kazakhstani, and ISTC funds. A new proposal to the Turkish Atomic Energy commission would enlarge the membership of our team.

References

[1] N. Burtebaev *et al.*, Phys. Rev. C **78**, 035802 (2008).

[2] N. Roughton *et al.*, At. Data Nucl. Data Tables **23**, 177 (1980).

5. Pion-induced Fission

R.J. Peterson (University of Colorado), Z. Yasin, and H.A. Kahn (Department of Nuclear Engineering, PIEAS, Islamabad, Pakistan)

Samples of Solid State Nuclear Track Detectors exposed to pion beams at the AGS are still being analyzed in Pakistan, and new cross sections are being determined. Several refereed publications

have appeared recently, and a review paper has been submitted for publication. An energetic Pakistani student is very active in this work, and we can expect yet more results. This student, Mr. Yasin, is also carrying out relevant theoretical computations using standard reaction codes

D. PUBLICATIONS AND REPORTS

Published Articles

We list here articles published for refereed journals, from the approximate date we closed the bibliography for our 2006 progress report. These are sorted by theme in order to make a more coherent list.

1. High Energy Deep-Inelastic Scattering and *pp* Reactions

These are results from the HERMES experiment (the HERMES collaboration including F. Ellinghaus, E.R. Kinney, and A. Martinez de la Ossa) at DESY focussed on nucleon structure, as well as results from the *pp* scattering reactions at RHIC (the PHENIX collaboration including F. Ellinghaus, E.R. Kinney, and J. Seele).

1. "Jet properties from dihadron correlations in p + p collisions at s**(1/2) = 200-GeV, " S.S. Adler *et al.*, Phys. Rev. D **74**, 072002 (2006).
2. "Longitudinal spin transfer to the Lambda hyperon in semi-inclusive deep-inelastic scattering," A. Airapetian *et al.*, Phys. Rev. D **74**, 072004 (2006).
3. "Measurement of high-p_T single electrons from heavy-flavor decays in p + p collisions at s**(1/2) = 200-GeV," A. Adare *et al.*, Phys. Rev. Lett. **97**, 252002 (2006).
4. "Measurement of direct photon production in p + p collisions at s**(1/2) = 200-GeV," S. S. Adler *et al.*, Phys. Rev. Lett. **98**, 012002 (2007).
5. "Precise determination of the spin structure function g_1 of the proton, deuteron and neutron," A. Airapetian *et al.*, Phys. Rev. D **75**, 012007 (2007).
6. "J/psi production vs transverse momentum and rapidity in p + p collisions at s**(1/2) = 200 GeV," Phys. Rev. Lett. **98**, 232002 (2007).
7. "Longitudinal-transverse separations of structure functions at low Q**2 for hydrogen and deuterium," V. Tvaskis *et al.*, Phys. Rev. Lett. **98**, 142301 (2007).
8. "Beam-spin asymmetries in the azimuthal distribution of pion electroproduction," A. Airapetian *et al.*, Phys. Lett. B **648**, 164 (2007).
9. "Inclusive cross section and double helicity asymmetry for π^0 production in p+p collisions at $\sqrt{s}$ = 200 GeV: Implications for the polarized gluon distribution in the proton," A. Adare *et al.*, Phys. Rev. D **76**, 051106 (2007).
10. "Transverse Polarization of Lambda and Lambda-bar Hyperons in Quasireal Photoproduction," , A. Airapetian *et al.*, Phys. Rev. D **76**, 092008 (2007).
11. "Evidence for a Transverse Single-Spin Asymmetry in Leptoproduction of $\pi^+\pi^-$ Pairs," A. Airapetian *et al.*, JHEP **0806**, 017 (2008).
12. "Measurement of Parton Distributions of Strange Quarks in the Nucleon from Charged-Kaon Production in Deep-Inelastic Scattering on the Deuteron," A. Airapetian *et al.*, Phys. Lett. B **666**, 446 (2008).
13. "Observation of the Naive-T-odd Sivers Effect in Deep-Inelastic Scattering," A. Airapetian *et al., Phys. Rev. Lett.* **103**, 152002 (2009).

14. "Dilepton mass spectra in $p + p$ collisions at $\sqrt{s}$ = 200 GeV and the contribution from open charm," A. Adare *et al., Phys. Lett.* **B670**, 313 (2009).

15. "Inclusive cross section and double helicity asymmetry for π^0 production in $p + p$ collisions at $\sqrt{s}$ = 62.4 GeV," A. Adare *et al., Phys. Rev.* **D79**, 012003 (2009).

16. "The polarized gluon contribution to the proton spin from the double helicity asymmetry in inclusive π^0 production in polarized $p + p$ collisions at $\sqrt{s}$ = 200 GeV," A. Adare *et al., Phys. Rev. Lett.* **103**, 012003 (2009).

17. "Applications of quark-hadron duality in F_2 structure function," S. P. Malace *et al., Phys. Rev.* **C80**, 035207 (2009).

18. "Double Helicity Dependence of Jet Properties from Dihadrons in Longitudinally Polarized $p + p$ Collisions at $\sqrt{s}$ = 200 GeV," A. Adare *et al., Phys. Rev.* **D81**, 012002 (2010).

19. "Transverse Momentum Dependence of J/ψ Polarization at midrapidity in $p + p$ Collisions at $\sqrt{s}$ = 200 GeV," A. Adare *et al., Phys. Rev.* **D82**, 012001 (2010).

20. "High p_T direct photon and π^0 triggered azimuthal jet correlations and measurement of k_T for isolated direct photons in $p + p$ collisions at *sqrts* = 200 GeV," A. Adare *et al., Phys. Rev.* **D82**, 072001 (2010).

21. "Leading-Order Determination of the Gluon Polarization from high-p_T Hadron Electroproduction," A. Airapetian *et al., JHEP* **1008**,130 (2010).

22. "Effects of Transversity in Deep-inelastic Scattering by Polarized Protons," A. Airapetian *et al., Phys. Lett.* **B693**, 11 (2010).

23. "Measurement of Transverse Single-Spin Asymmetries for J/ψ Production in Polarized $p+p$ Collisions at $\sqrt{s}$ = 200 GeV," A. Adare *et al., Phys. Rev.* **D82**, 112008 (2010);
Erratum *ibid.* **D86**, 099904 (2012).

24. "Search for a Two-Photon Exchange Contribution to Inclusive Deep-Inelastic Scattering," A. Airapetian *et al., Phys. Lett.* **B682**, 351 (2010).

25. "The proton and deuteron F_2 structure function at low Q^2," V. Tvaskis *et al., Phys. Rev.* **C81**, 055207 (2010).

26. "Inclusive Measurements of Inelastic Electron and Positron Scattering from Unpolarized Hydrogen and Deuterium Targets," A. Airapetian *et al., JHEP* **1105**, 126 (2011).

27. "Measurement of neutral mesons in $p+p$ collisions at $\sqrt{s}$ = 200 GeV and scaling properties of hadron production," A. Adare *et al., Phys. Rev.* **D83**, 052004 (2011).

28. "Cross Section and Parity Violating Spin Asymmetries of $W^{\pm}$ Boson Production in Polarized $p + p$ Collisions at $\sqrt{s}$ = 500 GeV," A. Adare *et al., Phys. Rev. Lett.* **106**, 062001 (2011).

29. "Event Structure and Double Helicity Asymmetry in Jet Production from Polarized $p + p$ Collisions at $\sqrt{s}$ = 200 GeV," A. Adare *et al., Phys. Rev.* **D84**, 012006 (2011).

30. "Cross section and double helicity asymmetry for η mesons and their comparison to neutral pion production in $p+p$ collisions at $\sqrt{s}$ = 200 GeV," A. Adare *et al., Phys. Rev.* **D83**, 032001 (2011).

31. "Identified charged hadron production in $p + p$ collisions at $\sqrt{s}$ = 200 and 62.4 GeV," A. Adare *et al., Phys. Rev.* **C83**, 064903 (2011).

32. "Ground and excited charmonium state production in $p + p$ collisions at $\sqrt{s}$ = 200 GeV," A. Adare *et al., Phys. Rev.* **D85**, 092004 (2012).

33. "Direct-Photon Production in $p+p$ Collisions at $\sqrt{s}$ = 200 GeV at Midrapidity," A. Adare *et al., Phys. Rev.* **D86**, 072008 (2012).

34. "Cross sections and double-helicity asymmetries of midrapidity inclusive charged hadrons in $p + p$ collisions at $\sqrt{s}$ = 62.4 GeV," A. Adare *et al., Phys. Rev.* **D86**, 092006 (2012).

35. "Measurement of the virtual-photon asymmetry A_2 and the spin-structure function g_2 of the proton," A. Airapetian *et al.,Eur. Phys. J.* **C72**, 1921 (2012).

2. Diffractive and Exclusive Reactions

Diffractive and Exclusive reactions at HERMES energies may be used to constrain the newly developed Generalized Parton Distributions.

1. "The beam-charge azimuthal asymmetry and deeply virtual Compton scattering," A. Airapetian *et al.*, Phys. Rev. D **75**, 011103 (2007).

2. "Recoil-Proton Polarization in High-Energy Deuteron Photodisintegration with Circularly Polarized Photons," X. Jiang *et al.,* Phys. Rev. Lett. **98**, 182302 (2007).

3. "Cross sections for hard exclusive electroproduction of π^+ mesons on a hydrogen target," A. Airapetian *et al.,* Phys. Lett. B **659**, 486 (2008).

4. "Measurement of Azimuthal Asymmetries With Respect To Both Beam Charge and Transverse Target Polarization in Exclusive Electroproduction of Real Photons," A. Airapetian *et al.,* JHEP **0806**, 066 (2008).

5. "Neutral Pion Electroproduction in the Resonance Region at High Q^2," A. N. Villano *et al., Phys. Rev.* **C80**, 035203 (2009)

6. "Spin Density Matrix Elements in Exclusive ρ^0 Electroproduction on ^{1}H and ^{2}H Targets at 27.5 GeV Beam Energy," A. Airapetian *et al., Eur. Phys. J.* **C62**, 659 (2009).

7. "Exclusive ρ^0 electroproduction on transversely polarized protons," A. Airapetian *et al., Phys. Lett.* **B679**, 100 (2009).

8. "Separation of contributions from deeply virtual Compton scattering and its interference with the Bethe–Heitler process in measurements on a hydrogen target," A. Airapetian *et al., JHEP* **0911**, 083 (2009).

9. "Single-spin azimuthal asymmetry in exclusive electroproduction of π^+ mesons on transversely polarized protons," A. Airapetian *et al., Phys. Lett.* **B682**, 345 (2010).

10. "Nuclear-mass dependence of azimuthal beam-helicity and beam-charge asymmetries in deeply virtual Compton scattering," A. Airapetian *et al., Phys. Rev.* **C81**, 035202 (2010).

11. "Measurement of azimuthal asymmetries associated with deeply virtual Compton scattering on an unpolarized deuterium target," A. Airapetian *et al., Nucl. Phys.* **B829**, 1 (2010).

12. "Exclusive Leptoproduction of Real Photons on a Longitudinally Polarized Hydrogen Target," A. Airapetian *et al., JHEP* **1006**, 019 (2010).

13. "Measurement of azimuthal asymmetries associated with deeply virtual Compton scattering on a longitudinally polarized deuterium target," A. Airapetian *et al., Nucl. Phys.* **B842**, 265 (2011).
14. "Ratios of Helicity Amplitudes for Exclusive ρ^0 Electroproduction," A. Airapetian *et al., Eur. Phys. J.* **C71**, 1609 (2011).
15. "Measurement of double-spin asymmetries associated with deeply virtual Compton scattering on a transversely polarized hydrogen target," A. Airapetian *et al., Phys. Lett.* **B704**, 15 (2011).
16. "Beam-helicity and beam-charge asymmetries associated with deeply virtual Compton scattering on the unpolarised proton," A. Airapetian *et al., JHEP* **1207**, 032 (2012).
17. "Beam-helicity asymmetry arising from deeply virtual Compton scattering measured with kinematically complete event reconstruction," A. Airapetian *et al., JHEP* **1210**, 042 (2012).

3. Nuclear Effects in High Energy Inelastic Scattering

Since the discovery of the EMC effect, there has been a steady program to understand the partonic nature of the nucleus. Recently this has expanded to include the use of the nucleus as a means to study the energy loss and hadronization of quarks as they evolve from fast quark to detected hadron. Studies at RHIC compare *d*-Au reactions to those in *pp* reactions at the same $\sqrt{s}$.

1. "Jet structure from dihadron correlations in d + Au collisions at s(NN)**(1/2) = 200-GeV," S.S. Adler *et al.*, Phys. Rev. C **73**, 054903 (2006).
2. "Centrality dependence of π^0 and η production at large transverse momentum in s_{NN}**(1/2) = 200 GeV d + Au collisions," S. S. Adler *et al.,* Phys. Rev. Lett. **98**, 172302 (2007).
3. "Production of Ω mesons at large transverse momenta in p + p and d + Au collisions at s_{NN}**(1/2) = 200 GeV," S. S. Adler *et al.,* Phys. Rev. C **75**, 051902 (2007).
4. "Hadronization in semi-inclusive deep-inelastic scattering on nuclei," A. Airapetian *et al.,* Nucl. Phys. B **780**, 1 (2007).
5. "Centrality dependence of charged hadron production in deuteron+gold and nucleon+gold collisions at $\sqrt{s_{NN}}$ = 200 GeV," S. S. Adler *et al.,* Phys. Rev. C **77**, 014905 (2008).
6. "Cold Nuclear Matter Effects on J/Ψ as Constrained by Deuteron-Gold Measurements at $\sqrt{s_{NN}}$ = 200 GeV," A. Adare *et al.,* Phys. Rev. C **77**, 024912 (2008).
7. "Transverse momentum broadening of hadrons produced in semi-inclusive deep-inelastic scattering on nuclei," A. Airapetian *et al., Phys. Lett.* **B684**, 114 (2010).
8. "Multidimensional Study of Hadronization in Nuclei," A. Airapetian *et al., Eur. Phys. J.* **A47**, 113 (2011).
9. "Cold Nuclear Matter Effects on *J*/ψ Yields as a Function of Rapidity and Nuclear Geometry in Deuteron-Gold Collisions at $\sqrt{s_{NN}}$ = 200 GeV," A. Adare *et al., Phys. Rev. Lett.* **107**, 142301 (2011).
10. "Suppression of back-to-back hadron pairs at forward rapidity in *d*+Au Collisions at $\sqrt{s_{NN}}$ = 200 GeV," A. Adare *et al., Phys. Rev. Lett.* **107**, 172301 (2011).

4. Relativistic Heavy Ion Physics

Our group supports the PHENIX experiment runs with heavy ions as well as polarized protons. While our focus is not on this physics, it is nonetheless interesting and we are especially excited by the possibility of understanding the parton energy loss by studying both the HERMES eA and PHENIX d-Au data.

1. "Scaling properties of azimuthal anisotropy in Au + Au and Cu + Cu collisions at s_{NN}**(1/2) = 200-GeV," A. Adare *et al.*, Phys. Rev. Lett. **98**, 162301 (2007).
2. "Correlated production of p and anti-p in Au + Au collisions at s_{NN}**(1/2) = 200-GeV," A. Adare *et al.*, Phys. Lett. B **649**, 359 (2007).
3. "Energy Loss and Flow of Heavy Quarks in Au+Au Collisions at sqrt(s_{NN}) = 200 GeV," A. Adare *et al.*, Phys. Rev. Lett. **98**, 172301 (2007).
4. "System size and energy dependence of jet-induced hadron pair correlation shapes in Cu + Cu and Au + Au collisions at s_{NN}**(1/2) = 200 GeV and 62.4 GeV," A. Adare *et al.*, Phys. Rev. Lett. **98**, 232302 (2007).
5. "J/ψ production vs centrality, transverse momentum, and rapidity in Au + Au collisions at s_{NN}**(1/2) = 200GeV," A. Adare *et al.*, Phys. Rev. Lett. **98**, 232301 (2007).
6. "Elliptic flow for φ mesons and (anti)deuterons in Au+Au collisions at $\sqrt{s_{NN}}$ = 200 GeV," S. Afanasiev *et al.*, Phys. Rev. Lett. **99**, 052301 (2007).
7. "Transverse momentum and centrality dependence of dihadron correlations in Au+Au collisions at $\sqrt{s_{NN}}$ = 200 GeV: Jet-quenching and the response of partonic matter," A. Adare *et al.*, Phys. Rev. C **77**, 011901 (2008).
8. "Source breakup dynamics in Au+Au Collisions at $\sqrt{s_{NN}}$ = 200 GeV via three-dimensional two-pion source imaging," S. Afanasiev *et al.*, Phys. Rev. Lett. **100**, 232301 (2008).
9. "Particle-species dependent modification of jet-induced correlations in Au+Au collisions at $\sqrt{s_{NN}}$ = 200 GeV," S. Afanasiev *et al.*, Phys. Rev. Lett. **101**, 082301 (2008).
10. "J/Ψ Production in $\sqrt{s_{NN}}$ = 200 GeV Cu+Cu Collisions," A. Adare *et al.*, Phys. Rev. Lett. **101**, 122301 (2008).
11. "Quantitative Constraints on the Opacity of Hot Partonic Matter from Semi-Inclusive Single High Transverse Momentum Pion Suppression in Au+Au collisions at $\sqrt{s_{NN}}$ = 200 GeV,", A. Adare *et al.*, Phys. Rev. C **77**, 064907 (2008).
12. "Dihadron azimuthal correlations in Au+Au collisions at $\sqrt{s_{NN}}$ = 200 GeV," A. Adare *et al.*, Phys. Rev. C **78**, 014901 (2008).
13. "Charged hadron multiplicity fluctuations in Au+Au and Cu+Cu collisions from $\sqrt{s_{NN}}$ = 22.5 to 200 GeV," A. Adare *et al.*, Phys. Rev. C **78**, 044902 (2008).
14. "Onset of π^0 Suppression Studied in Cu+Cu Collisions at $\sqrt{s_{NN}}$ = 22.4, 62.4, and 200 GeV," A. Adare *et al.*, Phys. Rev. Lett. **101**, 162301 (2008).
15. "Suppression pattern of neutral pions at high transverse momentum in Au + Au collisions at $\sqrt{s_{NN}}$ = 200 GeV and constraints on medium transport coefficients," A. Adare *et al.*, *Phys. Rev. Lett.* **101**, 232301 (2008).

16. "Dihadron azimuthal correlations in Au + Au collisions at $\sqrt{s_{NN}}$ = 200 GeV," A. Adare *et al., Phys. Rev.* **C78**, 014901 (2008).

17. "Charged hadron multiplicity fluctuations in Au + Au and Cu + Cu collisions from $\sqrt{s_{NN}}$ = 22.5 to 200 GeV," A. Adare *et al., Phys. Rev.* **C78**, 044902 (2008).

18. "Photoproduction of J/ψ and of high mass e^+e^- in ultra-peripheral Au+Au collisions at $\sqrt{s_{NN}}$ = 200 GeV," S. Afanasiev *et al., Phys. Lett.* **B679**, 321 (2009).

19. "Photon-Hadron Jet Correlations in $p + p$ and Au + Au Collisions at $\sqrt{s_{NN}}$ = 200 GeV," A. Adare *et al., Phys. Rev.* **C80**, 024908 (2009).

20. "Systematic Studies of Elliptic Flow Measurements in Au + Au Collisions at $\sqrt{s_{NN}}$ = 200 GeV," S. Afanasiev *et al., Phys. Rev.* **C80**, 024909 (2009).

21. "Measurement of Bottom versus Charm as a Function of Transverse Momentum with Electron-Hadron Correlations in $p + p$ Collisions at $\sqrt{s}$ = 200 GeV," A. Adare *et al., Phys. Rev. Lett.* **103**, 082002 (2009).

22. "Kaon interferometric probes of space-time evolution in Au + Au collisions at $\sqrt{s_{NN}}$ = 200 GeV," S. Afanasiev *et al.,Phys. Rev. Lett.* **103**, 142301 (2009).

23. "High-p_T π^0 Production with Respect to the Reaction Plane in Au + Au Collisions at $\sqrt{s_{NN}}$ = 200 GeV," S. Afanasiev *et al., Phys. Rev.* **C80**, 054907 (2009).

24. "Detailed measurement of the e^+e^- pair continuum in $p + p$ and Au + Au collisions at $\sqrt{s_{NN}}$ = 200 GeV and implications for direct photon production," A. Adare *et al., Phys. Rev.* **C81**, 034911 (2010).

25. "Enhanced production of direct photons in Au+Au collisions at $\sqrt{s_{NN}}$ = 200 GeV and implications for the initial temperature," A. Adare *et al., Phys. Rev. Lett.* **104**, 132301 (2010).

26. "Trends in Yield and Azimuthal Shape Modification in Dihadron Correlations in Relativistic Heavy Ion Collisions," A. Adare *et al., Phys. Rev Lett.* **104**, 252301 (2010).

27. "Elliptic and hexadecapole flow of charged hadrons in Au+Au collisions at $\sqrt{s_{NN}}$ = 200 GeV," A. Adare *et al., Phys. Rev. Lett.* **105**, 062301 (2010).

28. "Transverse momentum dependence of η meson suppression in Au+Au collisions at $\sqrt{s_{NN}}$ = 200 GeV," A. Adare *et al., Phys. Rev.* **C82**, 011902 (2010).

29. "Azimuthal anisotropy of neutral pion production in Au+Au collisions at $\sqrt{s_{NN}}$ = 200 GeV: Path-length dependence of jet quenching and the role of initial geometry," A. Adare *et al., Phys. Rev. Lett.* **105**, 142301 (2010).

30. "Nuclear modification factors of φ mesons in *d*+Au, Cu+Cu and Au+Au collisions at $\sqrt{s_{NN}}$ = 200 GeV," A. Adare *et al., Phys. Rev.* **C83**, 024909 (2011).

31. "Heavy Quark Production in $p+p$ and Energy Loss and Flow of Heavy Quarks in Au+Au Collisions at $\sqrt{s_{NN}}$ = 200 GeV," A. Adare *et al., Phys. Rev.* **C84**, 044905 (2011).

32. "Suppression of away-side jet fragments with respect to the reaction plane in Au+Au collisions at $\sqrt{s_{NN}}$ = 200 GeV," A. Adare *et al., Phys. Rev.* **C84**, 024904 (2011).

33. "Azimuthal correlations of electrons from heavy-flavor decay with hadrons in $p+p$ and Au+Au collisions at $\sqrt{s_{NN}}$ = 200 GeV," A. Adare *et al., Phys. Rev.* **C83**, 044912 (2011).

34. "*J*/ψ suppression at forward rapidity in Au+Au collisions at $\sqrt{s_{NN}}$ = 200 GeV," A. Adare *et al., Phys. Rev.* **C84**, 054912 (2011).

35. "Production of ω mesons in *p* + *p*, d+Au, Cu+Cu, and Au+Au collisions at $\sqrt{s_{NN}}$ = 200 GeV," A. Adare *et al., Phys. Rev.* **C84**, 044902 (2011).

36. "Measurements of Higher-Order Flow Harmonics in Au+Au Collisions at $\sqrt{s_{NN}}$ = 200 GeV," A. Adare *et al., Phys. Rev. Lett.* **107**, 252301 (2011).

37. "Observation of direct-photon collective flow in $\sqrt{s_{NN}}$ = 200 GeV Au+Au collisions," A. Adare *et al., Phys. Rev. Lett.* **109**, 122302 (2012).

38. "Deviation from quark-number scaling of the anisotropy parameter v_2 of pions, kaons, and protons in Au+Au collisions at $\sqrt{s_{NN}}$ = 200 GeV," A. Adare *et al., Phys. Rev.* **C85**, 064914 (2012).

39. "Nuclear-Modification Factor for Open-Heavy-Flavor Production at Forward Rapidity in Cu+Cu Collisions at $\sqrt{s_{NN}}$ = 200 GeV," A. Adare *et al., Phys. Rev.* **C86**, 024909 (2012).

40. "Evolution of π^0 suppression in Au+Au collisions from $\sqrt{s_{NN}}$ = 39 to 200 GeV," A. Adare *et al., Phys. Rev. Lett.* **109**, 152301 (2012).

41. "Measurement of Direct Photons in Au+Au Collisions at $\sqrt{s_{NN}}$ = 200 GeV," S. Afanasiev *et al., Phys. Rev. Lett.* **109**, 152302 (2012).

42. "*J*/ψ suppression at forward rapidity in Au+Au collisions at $\sqrt{s_{NN}}$ = 39 and 62.4 GeV," A. Adare *et al., Phys. Rev.* **C86**, 064901 (2012).

5. Incoherent Nuclear Reactions

We have combined our interests in nucleon structure and dynamics with our history of reactions on complex nuclei to develop and continue a program to study quasifree scattering of hadrons from complex nuclei to examine incoherent hadron-nucleon interactions within the nuclear medium.

1. "Nuclear Continuum Scattering of Hadrons at $x_B > 1$, R.J. Peterson, Nucl. Phys. A **791** 84 (2007).
2. "Nuclear Continuum Charge Exchange of hadrons at $x_B > 1$, R.J. Peterson, Nucl. Phys. A **803**, 46 (2008).
3. "Unification of intermediate energy hadron spectra with small energy losses," R.J. Peterson, Proc. Int. Conf. on Nuclear Data for Science and Technology, Nice, France April 22-27, 2007, EDP Sciences, p. 1141-1142 (2008).
4. "Scaling relations for Intermediate Energy Proton-Nucleus Reactions with Small Energy Losses," R.J. Peterson, Nucl. Sci. Engin. 161, 346-356 (2009).

5. "*y*-scaling in hadronic continuum spectra,' R.J.!Peterson, in *Nuclear Theory*, Inst. for Nuclear Research and Nuclear Energy, Bulgarian Academy of Sciences, S. Dimitrova, ed., 123 (2009).

6. Meson Reaction Mechanisms

Although our experimental program with intermediate energy meson beams is complete, data analysis has continued to publication.

1. "Inclusive pion double charge exchange in light *p*-shell nuclei," W. Fong, J.L. Matthews, M.L. Dowell, E.R. Kinney, T. Soos, M.Y. Wang, S.A. Wood, P.A.M. Gram, G.A. Rebka, Jr., D.A. Roberts, Phys. Rev. C **75**, 064605 (2007).
2. "Differential cross sections of the charge-exchange reaction $\pi^- p \rightarrow \pi^0 n$ in the momentum range from 103 to 178 MeV/c," D. Mekterovic *et al.,* Phys. Rev. C **80**, 055207 (2009).

7. Miscellaneous

We continue to include a broad range of activities in nuclear science including some based on older interests.

1. "Energy dependence of fission probabilities induced by negative pions in Sn, Au and Bi," M.I. Shahzad, Z. Yasin, R.J. Peterson, G. Sher, M.T. Javed and H.A. Khan, Nucl. Phys. **A781** 296 (2007).
2. "Comparison of fission induced by nucleons and pions," Z. Yasin, R.J. Peterson, M.I. Shahzad and H.A. Khan, Proc. Int. Conf. on Nuclear Data for Science and Technology, Nice, France, April 22-27, 2007, EDP Sciences, p. 1137-1139 (2008).
3. "Theoretical study and systematic analysis of positive pion-induced fission cross sections of heavy nuclei," Z. Yasin, M.I. Shazad, H.A. Khan, R.J. Peterson and M. Asghar, Radiation Measurements **43**, 174 (2008).
4. "Energy dependence of negative pion-induced fission of tin," H.A. Khan, M.I. Shahzad, Z. Yasin, I.E. Qureshi, G. Sher, S. Manzoor and R.J. Peterson, Radiation Measurements **43**, 188 (2008).
5. "Nuclear Fission Induced by Pi Mesons," R.J. Peterson, Journal of Nuclear and Radiochemical Sciences, **11** 63 (2010).
6. "New $^{12}C(p,\gamma)$ radiative capture measurements," N. Burtebaev, *et al.,* Phys. Rev. C **78**, 035802 (2008).
7. "New measurements of the astrophysical S-factor for the $^{12}C(p,\gamma)^{13}N$ reaction at low energies and the asymptotic normalization coefficient (nuclear vertex constant) for the $p + ^{12}C \rightarrow ^{13}N$ reaction," N. Burtebaev, S.B. Igamov, R.J. Peterson, R. Yarmukhamedov and D.M. Zazulin, Phys. Rev. C **78**, 035802 (2008).
8. "Charged kaon mass measurement using the Cherenkov effect," N. Graf *et al.*al., Nucl. Instr. Meth. **A615**, 27 (2010).
9. "How to Develop Scientists in the Developing World," R.J. Peterson, in 'Basic or Applied Research: Dilemma of Developing Countries', Ed. H.A. Khan, M.M. Qureshi and I. Hayee, COMSATS, Islamabad, Pakistan, 161-168 (2007).
10. "Collaborating for Success," R.J. Peterson, in "Science and Technology Policies and Strategies for Sustainable Development," Ed. H.A. Khan, COMSATS, Islamabad, Pakistan (2008).
11. "New Nukes for New Niches," R.J. Peterson, Whitehead Journal of Diplomacy and International Relations, **11**, 75 (2010).

8. Conference Presentations

We list here presentations made at conferences and workshops since the approximate date we closed the bibliography for our 2006 progress report; the order is simply chronological. We have not included seminars, colloquia, and other public presentations and outreach.

1. "Quark Orbital Angular Momentum and Exclusive Processes at HERMES," F. Ellinghaus [HERMES Collaboration], 9th Conference on the Intersections of Nuclear and Particle Physics (CIPANP2006), Rio Grande, Puerto Rico, May 30 - Jun 3, 2006, AIP Conf. Proc. **870** 615 (2006).
2. "Double Helicity Asymmetry and Cross Section for η Production in Polarized pp Collisions at PHENIX," F. Ellinghaus [PHENIX Collaboration], 17th Int. Spin Physics Symp. (SPIN2006), Kyoto, Japan, October 2-7, 2006, AIP Conf. Proc. **915** 363 (2007).
3. "New Results on ρ^0 Production at HERMES," E.R. Kinney [HERMES Collaboration], 17th Int. Spin Physics Symp. (SPIN2006), Kyoto, Japan, October 2-7, 2006.
4. "J/psi Measurements in $sqrts_{NN}$=200 GeV Au + Au Collisions," A.M. Glenn [PHENIX Collaboration], Fall Meeting of the APS Division of Nuclear Physics, Nashville, TN, October 25-28, 2006.
5. "The η double helicity asymmetry and cross section," J. Seele [PHENIX Collaboration], Fall Meeting of the APS Division of Nuclear Physics, Nashville, TN, October 25-28, 2006.
6. "Realisitic Simulation of W Boson production in the PHENIX Muon Spectrometers," K.G. Kiriluk [PHENIX Collaboration], , Fall Meeting of the APS Division of Nuclear Physics, Nashville, TN, October 25-28, 2006.
7. "Probing $x = \xi$ through DVCS spin observables at HERMES, Probing $x * \xi$ through the DVCS beam charge asymmetry, and 'First' experimental results for DVCS on Nuclei," F. Ellinghaus [HERMES Collaboration], Workshop on Hard exclusive processes at JLab 12 GeV and at a future EIC, College Park, MD, October 29-30, 2006.
8. "PHENIX results for J/ψ transverse momentum and rapidity dependence in *Au+Au* and *Cu+Cu* collisions," (Invited) A.M. Glenn [PHENIX Collaboration], Quark Matter, Int. Conf. Ultra-Rel. Nucl.-Nucl. Coll. Shanghai, China, November 14-20, 2006, A.M. Glenn *et al.,* J. Phys. G **34** S737 (2007).
9. "The PHENIX Resistive Plate Chamber Forward Upgrades," A.M. Glenn [PHENIX Collaboration], Winter Workshop on Nuclear Dynamics, Big Sky, MT, February 11-18, 2007.
10. "Simulation of Semi-inclusive DIS from Polarized ep Collisions at Proposed EIC energies," J. Seele and E. Kinney, Spring Meeting of the American Physical Society, Jacksonville, FL, April 14-17, 2007.
11. "Scaling relations among hadron continuous spectra," R.J. Peterson, Int. Conf. on Nuclear Data for Science and Technology (ND2007), Nice, France, April 22-27, 2007.
12. "Semi-inclusive Deep Inelastic Scattering at HERMES and at the proposed EIC," (invited) E.R. Kinney, RIKEN-BNL Workshop on Parity-Violating Spin Asymmetries at RHIC, Upton, NY April 26-27, 2007.

13. "DVCS at HERMES," F. Ellinghaus [HERMES Collaboration], Workshop on Exclusive Reactions at High Momentum Transfer, Jefferson Lab, Newport News, VA, May 21-24, 2007.

14. "PHENIX Spin Physics Overview," F. Ellinghaus [PHENIX Collaboration], 11th Int. Conf. on Baryons (BARYON07), Seoul, Korea, June 11-15, 2007.

15. "Scaling relations among (p,nx) and (p, px) continuous spectra at intermediate energies," R.J. Peterson, 8th Int. Topical Meeting on Nuclear Applications and Utilization of Accelerators, Pocatello, ID, July 30 - August 2, 2007.

16. "GPD and TMD Studies at HERMES," (invited) F. Ellinghaus [HERMES Collaboration], Fall Meeting of the APS Division of Nuclear Physics, Newport News, VA October 10-13, 2007.

17. "Parameterization of the η Fragementation Functions from World e+e- and p+p data," C. Aidala, J. Seele, M. Stratmann, and W. Vogelsang, Fall Meeting of the APS Division of Nuclear Physics, Newport News, VA, October 10-13, 2007.

18. "HERMES Measurement of the Collins and Sivers Asymmetries from a Transversely Polarized Hydrogen Target," E. Kinney [HERMES Collaboration], Fall Meeting of the APS Division of Nuclear Physics, Newport News, VA, October 10-13, 2007.

19. "Recent PHENIX Results on π^+, π^-, and η Production in polarized pp Collisions at RHIC at $\sqrt{s}$ = 200 GeV," F. Ellinghaus [PHENIX Collaboration], 16th Int. Workshop on Deep Inelastic Scattering and Related Subjects (DIS 2008), London, England, April 7-11, 2008.

20. "Constraining the polarized gluon PDF in $p\,p$ collisions at RHIC," F. Ellinghaus [PHENIX and STAR Collaborations], 34th Int. Conf. on High Energy Physics (ICHEP08), Philadelphia, USA, July 29 - August 5, 2008.

21. "Review of ΔG programs in DIS and $p\,p$," F. Ellinghaus [PHENIX and STAR Collaborations], 18th Int. Symp. on Spin Physics, Charlottesville, USA, October 6-11, 2008, AIP Conf. Proc. **1149**, 259 (2009).

22. "What Can We Learn from η Production in $p - p$ Collisons at PHENIX," J. Seele [PHENIX Collaboration], 18th Int. Symp. on Spin Physics, Charlottesville, USA, October 6-11, 2008., AIP Conf. Proc. **1149**, 568 (2009).

23. "Drell-Yan Measurements of Light Antiquarks in the Nucleon and in Nuclei," 18th Int. Conf. on Particles and Nuclei (PANIC08), Eilat, Israel, Nov. 9-14, 2008, *Nucl. Phys.* **A827**, 330 (2009).

24. "Systematics of local pion optical model parameters," D.R. Sarker, F. Khanam, H.M. Sengupta and R.J. Peterson, Proc. 12th International Conference on Nuclear Reaction Mechanisms, ed. F. Cerutti and A. Ferrari, 211 (2010).

E. LABORATORY PERSONNEL

1. Academic and Scientific

F. Ellinghaus[1]	Research Associate
A. Martinez de la Ossa[2]	Research Associate
J. Katich[3]	Research Associate
E.R. Kinney	Professor
R.J. Peterson	Professor

2. Technical and Support Staff

S. Spika	Administrative Assistant
E. Erdos	Professional Research Assistant

3. Research Assistants

J. Nuger[4]
J. Seele[5]
P.-J. Lin[6]

4. Undergraduate Research Assistants

C. West	January 2009 - May 2010
J. Braverman	June 2009 - July 2010
D. Sprinzen	January 2010 - August 2010
S. MacCoun	January 2010 - August 2010
R. Lewis	September 2010 - May 2011
B. MacDonald	September 2012 - November 2013

[1]Appointment ended August 2008
[2]Appointment began May 2008, ended September 2010
[3]Appointment began September 2010
[4]Graduated with M.S. December 2009
[5]Graduated with Ph.D. December 2008
[6]Matriculated at University of Colorado August 2009, appointed August 2009